

# Gadolinium Complexes of Highly Rigid, Open-Chain Ligands Containing a Cyclobutane Ring in the Backbone: Decreasing Ligand Denticity Might Enhance Kinetic Inertness

Oriol Porcar-Tost,<sup>†</sup> José A. Olivares,<sup>†</sup> Agnès Pallier,<sup>‡</sup> David Esteban-Gómez,<sup>§</sup> Ona Illa,<sup>†</sup> Carlos Platas-Iglesias,<sup>\*,§</sup> Éva Tóth,<sup>\*,‡</sup> and Rosa M. Ortuño<sup>\*,†</sup>

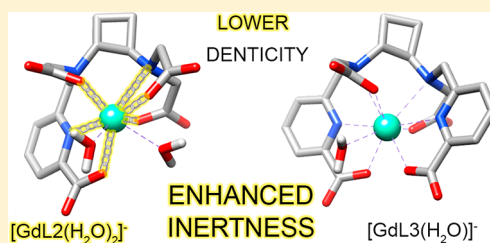
<sup>†</sup>Departament de Química, Universitat Autònoma de Barcelona, 08193 Cerdanyola del Vallès, Barcelona, Spain

<sup>‡</sup>Centre de Biophysique Moléculaire, UPR 4301, CNRS, Université d'Orléans, rue Charles Sadron, 45071 Orléans Cedex 2, France

<sup>§</sup>Centro de Investigaciones Científicas Avanzadas and Departamento de Química, Universidade da Coruña, Campus da Zapateira-Rúa da Fraga 10, 15008 A Coruña, Spain

## Supporting Information

**ABSTRACT:** In an effort to explore novel ligand scaffolds for stable and inert lanthanide complexation in magnetic resonance imaging contrast agent research, three chiral ligands containing a highly rigid (1*S*,2*S*)-1,2-cyclobutanediamine spacer and different number of acetate and picolinate groups were efficiently synthesized. Potentiometric studies show comparable thermodynamic stability for the Gd<sup>3+</sup> complexes formed with either the octadentate (L3)<sup>4−</sup> bearing two acetate or two picolinate groups or the heptadentate (L2)<sup>4−</sup> analogue bearing one picolinate and three acetate groups (log *K*<sub>GdL</sub> = 17.41 and 18.00 for [Gd(L2)]<sup>−</sup> and [Gd(L3)]<sup>−</sup>, respectively). In contrast, their dissociation kinetics is revealed to be very different: the monohydrated [Gd(L3)]<sup>−</sup> is considerably more labile, as a result of the significant kinetic activity of the protonated picolinate function, as compared to the bishydrated [Gd(L2)]<sup>−</sup>. This constitutes an uncommon example in which lowering ligand denticity results in a remarkable increase in kinetic inertness. Another interesting observation is that the rigid ligand backbone induces an unusually strong contribution of the spontaneous dissociation to the overall decomplexation process. Thanks to the presence of two inner-sphere water molecules, [Gd(L2)]<sup>−</sup> is endowed with high relaxivity (*r*<sub>1</sub> = 7.9 mM<sup>−1</sup> s<sup>−1</sup> at 20 MHz, 25 °C), which is retained in the presence of large excess of endogenous anions, excluding ternary complex formation. The water exchange rate is similar for [Gd(L3)]<sup>−</sup> and [Gd(L2)]<sup>−</sup>, while it is 1 order of magnitude higher for the trishydrated tetraacetate analogue [Gd(L1)]<sup>−</sup> (*k*<sub>ex</sub><sup>298</sup> = 8.1, 10, and 127 × 10<sup>6</sup> s<sup>−1</sup>, respectively). A structural analysis via density functional theory calculations suggests that the large bite angle imposed by the rigid (1*S*,2*S*)-1,2-cyclobutanediamine spacer could allow the design of ligands based on this scaffold with suitable properties for the coordination of larger metal ions with biomedical applications.



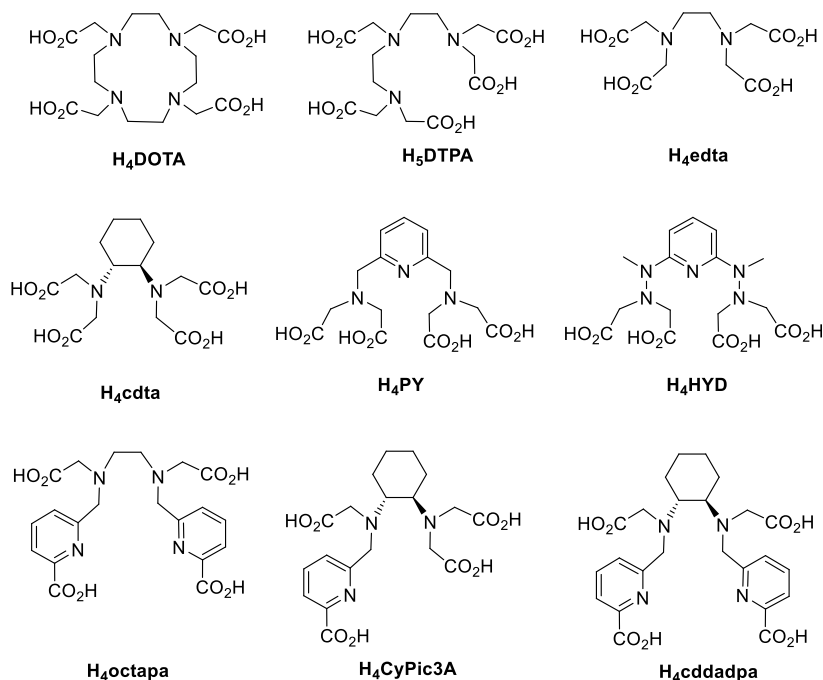
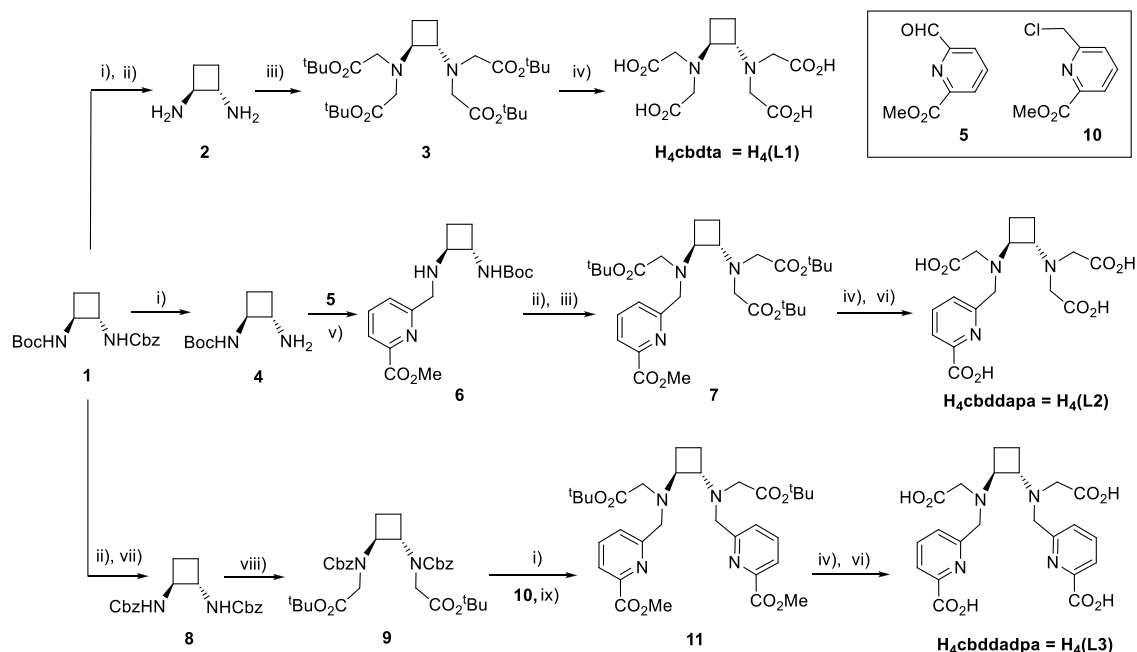
## INTRODUCTION

Contrast agents (CA) are paramagnetic or super-paramagnetic substances that improve the sensitivity and the specificity of magnetic resonance imaging (MRI) examinations. In the last decades, there has been very active research to design more efficient, selective, and safer CAs, which are valuable tools in preclinical imaging, clinical diagnosis, and, more recently, in theranostic approaches.<sup>1</sup> Given its seven unpaired electrons and slow electron spin relaxation, paramagnetic Gd<sup>3+</sup> has the greatest effect on nuclear relaxation times of surrounding nuclei and is the most-used metal ion in MRI contrast agents. To prevent in vivo toxicity of the complexes, which would be related to the release of the free, noncomplexed metal, Gd<sup>3+</sup> needs to be chelated in complexes of high thermodynamic stability and kinetic inertness that ensure stable complexation at physiological pH.<sup>2</sup> Several mechanisms account for the possible dissociation of Gd<sup>3+</sup> complexes. These involve spontaneous and acid-catalyzed processes, as well as dissociation assisted by endogenous metal ions, such as Zn<sup>2+</sup>

and Cu<sup>2+</sup>. Typically, complexes formed with macrocyclic ligands are kinetically more inert than the linear analogues,<sup>3</sup> and their dissociation mechanisms are also different. Whereas the acid-catalyzed pathway is the major contributor to the dissociation of macrocyclic chelates (Chart 1),<sup>4</sup> linear complexes tend to dissociate via metal-assisted pathways.<sup>2a,5</sup> For example, transmetalation reactions between [Gd(DTPA-BMA)] and Cu<sup>2+</sup> in the presence of citrate, phosphate, and bicarbonate anions occur through dissociation of the gadolinium complex assisted by endogenous ligands.<sup>5</sup> Previous work has shown that the incorporation of rigid moieties in the structure of linear ligands results in significantly improved kinetic inertness of their lanthanide complexes. A remarkable example is the highly rigid [Gd(cddadpa)]<sup>−</sup> complex (Chart 1). It presents not only good thermodynamic stability but also a kinetic inertness that is unprecedented for a linear ligand,

Received: July 9, 2019

Chart 1. Previously Reported Ligands Related to Those Described and Studied in This Work

Scheme 1. Synthesis of Ligands H<sub>4</sub>cbdt, H<sub>4</sub>cbddadpa, and H<sub>4</sub>cbddadpa (H<sub>4</sub>(L1), H<sub>4</sub>(L2), and (H<sub>4</sub>L3))<sup>a</sup>

<sup>a</sup>Reagents and conditions: (i) H<sub>2</sub>, Pd(OH)<sub>2</sub>, CH<sub>3</sub>OH, rt, 84%; (ii) (a) 2 M HCl in diethyl ether, CH<sub>2</sub>Cl<sub>2</sub>, rt, 4 h; (b) K<sub>2</sub>CO<sub>3</sub>, CH<sub>2</sub>Cl<sub>2</sub>, rt, 2 h, 80%; (iii) *tert*-butyl bromoacetate, KI, DIPEA, DMF, rt, 18 h, 74%; (iv) 4 M HCl in dioxane, rt, 18 h, 77%; (v) (a) MeOH, rt, 2.5 h; (b) NaBH<sub>4</sub>, CH<sub>3</sub>OH, 0 °C, 2 h, 87%; (vi) LiOH, 1:1 THF–H<sub>2</sub>O, rt, 4 h, quantitative; (vii) ClCO<sub>2</sub>Bn, NaHCO<sub>3</sub>, Na<sub>2</sub>CO<sub>3</sub>, 7:1 H<sub>2</sub>O–acetone, 0 °C, 18 h, 60%; (viii) TBAI, NaH, THF, rt, 18 h, 62%; (ix) KI, DIPEA, DMF, rt, 30 h, 57%.

being comparable to those of clinically approved macrocyclic complexes.<sup>6</sup>

In the design of novel MRI agents, in addition to safety issues, one must also consider the structural parameters that affect the proton relaxivity  $r_1$  and, thus, the efficiency of a CA. Indeed, relaxivity is related to a number of microscopic parameters of the paramagnetic chelate as described by the Solomon-Bloembergen-Morgan (SBM) theory of paramag-

netic relaxation,<sup>7</sup> the most important being the number of hydration water molecules ( $q$ ), the water exchange rate, the rotational dynamics of the complex, and its electron spin relaxation.

Relaxivity is linearly proportional to the number of inner-sphere water molecules; however, complexes with high hydration numbers are often thermodynamically less stable, increasing the risk of metal release. Moreover, for bishydrated

**Table 1. Protonation Constants of (L1)<sup>4−</sup>, (L2)<sup>4−</sup>, (L3)<sup>4−</sup>, and Related Ligands, and Stability Constants of Their Metal Complexes (25 °C, 0.15 M KCl)**

	(L1) <sup>4−</sup>	(L2) <sup>4−</sup>	(L3) <sup>4−</sup>	edta <sup>4− 11</sup>	cdta <sup>4−</sup>	octapa <sup>4− 2h</sup>	cddadpa <sup>4− 6</sup>
log K <sub>1</sub> <sup>H</sup>	9.66 ± 0.01	9.58 ± 0.02	8.89 ± 0.03	9.18	9.36 <sup>12</sup>	8.52	9.35
log K <sub>2</sub> <sup>H</sup>	5.84 ± 0.01	6.00 ± 0.04	6.61 ± 0.03	6.00	5.95 <sup>12</sup>	5.40	5.66
log K <sub>3</sub> <sup>H</sup>	3.06 ± 0.02	3.78 ± 0.04	4.26 ± 0.06	2.58	3.62 <sup>12</sup>	3.65	4.20
log K <sub>4</sub> <sup>H</sup>	2.08 ± 0.03	2.32 ± 0.05	2.97 ± 0.06	2.29	2.57 <sup>12</sup>	2.97	3.72
log K <sub>5</sub> <sup>H</sup>	1.71 ± 0.08	2.07 ± 0.05	2.79 ± 0.06		1.49 <sup>12</sup>	1.66	2.62
Σlog K <sub>i</sub> <sup>H</sup>	22.35	23.75	25.52	20.05	22.99 <sup>12</sup>	22.20	25.55
log K <sub>GdL</sub>	14.73 ± 0.01	17.41 ± 0.01	18.00 ± 0.02 <sup>b</sup>	16.28	18.97 <sup>13</sup>	20.23	20.68
log K <sub>GdHL</sub>	2.38 ± 0.03	2.36 ± 0.02	3.28 ± 0.03 <sup>b</sup>		1.66 <sup>13</sup>		2.38
log K <sub>ZnL</sub>	12.26 ± 0.01	15.22 ± 0.01	16.28 ± 0.05	14.61	16.75 <sup>14</sup>	19.32	15.85
log K <sub>ZnHL</sub>	4.10 ± 0.01	3.78 ± 0.01	4.00 ± 0.04		2.57 <sup>14</sup>		3.81
log K <sub>ZnH2L</sub>			3.41 ± 0.04				
pGd <sup>a</sup>	13.4	16.2	17.4	15.4	18.0	20.0	19.7

<sup>a</sup>pGd = −log[Gd<sup>3+</sup><sub>free</sub>] at c<sub>L</sub> = 1 × 10<sup>−5</sup> M; c<sub>Gd</sub> = 1 × 10<sup>−6</sup> M; pH 7.4. <sup>b</sup>With La: log K<sub>LaL</sub> = 18.74 ± 0.01 and log K<sub>LaHL</sub> = 2.8 ± 0.1; with Lu: log K<sub>LuL</sub> = 17.02 ± 0.01 and log K<sub>LuHL</sub> = 3.85 ± 0.1.

chelates, the coordinated water molecules can be replaced by endogenous anions, thereby decreasing the efficiency of the CA.<sup>8</sup> Usually, complexes with more than one hydration water also present lower kinetic inertness, although it has been observed that the incorporation of cyclohexane or pyridine moieties, for instance, in [Gd(CyPic3A)]<sup>−</sup> or [Gd(HYD)]<sup>−</sup>, respectively, leads to a remarkable kinetic inertness for these bishydrated complexes, which is comparable to that of the monohydrated [Gd(DTPA)]<sup>2−</sup> (Chart 1).<sup>9</sup> Furthermore, lowering the ligand basicity, for example, with hydrazine functions in [Gd(HYD)]<sup>−</sup>, was also identified as an important factor to improve kinetic inertness.<sup>9b</sup>

In the objective of inducing ligand rigidity, we incorporated a cyclobutane ring in the scaffold of linear chelators. Here we present the synthesis of three new ligands, H<sub>4</sub>cbddta, H<sub>4</sub>cbddapa, and H<sub>4</sub>cbddadpa, that will be referred to as H<sub>4</sub>(L1), H<sub>4</sub>(L2), and H<sub>4</sub>(L3), respectively (Scheme 1; see Experimental Section for full names), and the investigation of their Gd<sup>3+</sup> complexes with respect to thermodynamic stability, kinetic inertness, and relaxometric properties. In addition to the assessment of the role of a highly rigid ligand backbone, the comparison of complexes [Gd(L1)]<sup>−</sup>, [Gd(L2)]<sup>−</sup>, and [Gd(L3)]<sup>−</sup> provides information about the influence of the picolinate moiety and of increasing ligand denticity on these properties. Indeed, (L1)<sup>4−</sup>, (L2)<sup>4−</sup>, and (L3)<sup>4−</sup> are potentially hexa-, hepta-, and octadentate, respectively; therefore, coordination of 3, 2, and 1 inner-sphere water molecules is expected in their Gd<sup>3+</sup> complexes. This experimental assessment was completed with density functional theory (DFT) calculations on [Gd(L2)]<sup>−</sup> and [Gd(L3)]<sup>−</sup> to gain further insight into the relationship between structure and coordination chemistry of these novel and highly rigid chelators.

## RESULTS AND DISCUSSION

### Synthesis of the Ligands and of the Gd<sup>3+</sup> Complexes.

Ligands H<sub>4</sub>(L1), H<sub>4</sub>(L2), and H<sub>4</sub>(L3) were synthesized according to Scheme 1, starting from chiral and orthogonally protected (1S,2S)-1,2-cyclobutanedi-amine, **1**, which was previously described.<sup>10</sup>

Sequential deprotection of diamine **1** by catalytic hydrogenolysis of the benzyl carbamate and acid hydrolysis of the *tert*-butyl carbamate afforded free diamine **2** at room temperature (rt) in 64% yield for the two steps. Alkylation of **2** with *tert*-butyl bromoacetate (4.4 equiv) in the presence of

diisopropylethyl amine (DIPEA) and potassium iodide led to **3**, which, by acidolysis of *tert*-butyl esters, provided H<sub>4</sub>(L1) in 54% yield for the two steps.

Alternatively, reductive amination of methyl 6-formylpicolinate, **5**, with amine **4** gave compound **6** in 87% yield. Subsequent removal of *tert*-butyl carbamate followed by alkylation led to **7** in 74% yield. Finally, saponification of the methyl ester with LiOH followed by acidolysis of the three *tert*-butyl esters afforded H<sub>4</sub>(L2) in 77% yield.

The synthetic route to H<sub>4</sub>(L3) was slightly different, since attempts to introduce the second picolinate unit by reductive amination, both in one-pot reaction and in a sequential manner, failed probably due to the severe steric constriction imposed by the cyclobutane ring. Neither the attempt to do it by alkylation of the second amine with methyl chloromethylpicolinate, **10**, was satisfactory. The order of introduction of the substituents by alkylation reactions was then reversed. Symmetric dicarbamate **8** was prepared in 60% yield from **1** by removal of the *tert*-butyl carbamate and reaction of the free amine with benzyl chloroformate. Compound **8** reacted with *tert*-butyl bromoacetate using NaH as a base and in the presence of tetrabutylammonium iodide (TBAI) in anhydrous tetrahydrofuran (THF) for 18 h. Compound **9** was then obtained in 62% yield. Hydrogenolysis of the benzyl carbamates and subsequent reaction with **10** led to **11** (57% yield), which, after full deprotection, provided H<sub>4</sub>(L3) in 70% yield.

[Gd(L1)]<sup>−</sup>, [Gd(L2)]<sup>−</sup>, and [Gd(L3)]<sup>−</sup> complexes were synthesized in aqueous solution by reaction of equimolar amounts of the corresponding ligand and GdCl<sub>3</sub>·6H<sub>2</sub>O followed by adjustment of the pH to ~7. The high-resolution mass spectrometry (HRMS) spectra of the complexes showed the expected peaks in each case confirming their formation (see the Supporting Information).

**Ligand Protonation Constants and Stability Constants of the Metal Complexes.** The protonation constants of (L1)<sup>4−</sup>, (L2)<sup>4−</sup>, and (L3)<sup>4−</sup>, as well as the stability constants of their complexes with Gd<sup>3+</sup> and Zn<sup>2+</sup>, were determined by pH-potentiometric titrations. For (L3)<sup>4−</sup>, the stability constants with La<sup>3+</sup> and Lu<sup>3+</sup> were also assessed. The global basicity of the three ligands increases in the order of (L1)<sup>4−</sup> < (L2)<sup>4−</sup> < (L3)<sup>4−</sup> (Table 1), in accordance with the subsequent incorporation of one and two picolinate units, respectively, in L2 and L3.

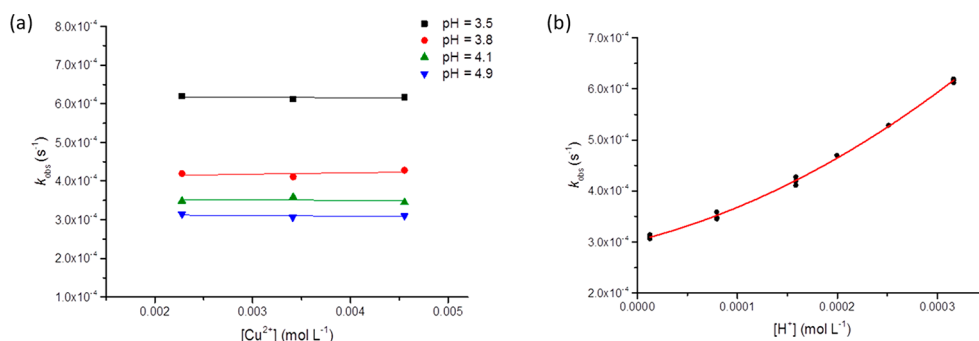


**Figure 1.** Plot of  $k_{\text{obs}}$  values for the dissociation of  $[\text{Gd}(\text{L2})]^-$  (0.1138 mM) as a function of the  $\text{Cu}^{2+}$  ion concentration at pH 3.5, 3.8, 4.1, and 4.9 (a) and as a function of proton concentration (b). The red line on (b) represents the fit to eq 1.

**Table 2.** Dissociation Rate Constants of  $[\text{Gd}(\text{L2})]^-$  and of Some Relevant  $\text{Gd}^{3+}$  Complexes Used as MRI Contrast Agents

ligand	(L2) <sup>4-</sup>	PY <sup>4-</sup> 15	HYD <sup>4-</sup> 9b	octapa <sup>4-</sup> 2h	cddadpa <sup>4-</sup> 6	DTPA <sup>4-</sup> 2a
$k_0$ [s <sup>-1</sup> ]	$3.0 \times 10^{-4}$					
$k_1$ [M <sup>-1</sup> s <sup>-1</sup> ]	0.49	0.17	0.85	11.8	0.016	0.58
$k_2$ [M <sup>-1</sup> s <sup>-1</sup> ]	$1.58 \times 10^3$	520	9.8	$2.5 \times 10^4$		$9.7 \times 10^4$
$k_3^{\text{Cu}}$ [M <sup>-1</sup> s <sup>-1</sup> ]			$2.4 \times 10^{-3}$	22.5	$6.8 \times 10^{-4}$	0.93
$t_{1/2}$ [h] <sup>a</sup>	0.64	$2.8 \times 10^4$	$5.3 \times 10^3$	0.15	$1.49 \times 10^5$	202

<sup>a</sup> $t_{1/2} = \ln 2 / k_{\text{obs}}$ , where  $k_{\text{obs}}$  was calculated by using pH 7.4 and  $c\text{Cu}^{2+} = 1 \mu\text{M}$ .

The first protonation constant ( $\log K_1$ ), corresponding to the protonation of a backbone nitrogen, is similar for (L1)<sup>4-</sup> (9.66) and (L2)<sup>4-</sup> (9.58), while it is smaller for (L3)<sup>4-</sup> (8.89). A similar tendency was observed for the tetraacetate edta<sup>4-</sup> (edta = ethylenediaminetetraacetic acid) with respect to the bispicolinate derivative octapa<sup>4-</sup> (octapa = 6,6'-[(ethane-1,2-diyl-bis((carboxymethyl)azanediyl))bis(methylene)]-dipicolinic acid), the latter having a considerably lower  $\log K_1$  value (8.52 vs 9.18).<sup>2h</sup> The rigidity of the ligand also affects the first protonation constant; with identical pending groups,  $\log K_1$  is typically higher for the rigidified ligands containing a cyclobutyl or a cyclohexyl moiety instead of the flexible ethylene bridge between the two amines (Table 1).

Ligands (L1)<sup>4-</sup>, (L2)<sup>4-</sup>, and (L3)<sup>4-</sup> form both non-protonated and monoprotonated mononuclear complexes with  $\text{Gd}^{3+}$  and  $\text{Zn}^{2+}$  ions. In addition, (L3)<sup>4-</sup> forms a diprotonated  $\text{Zn}^{2+}$  complex as well. These protonated complexes are observed at acidic pH (see species distribution diagrams in Supporting Information) and can be attributed to the protonation of the carboxylate groups. At pH 7, only the nonprotonated complexes exist for any of the three systems. Above pH 10, a slight precipitation was observed in the  $[\text{Gd}(\text{L1})]^-$  and  $[\text{Gd}(\text{L2})]^-$  samples, possibly due to the formation of hydroxo complexes. The stability constants of those complexes could not be calculated, and therefore only experimental data below that point were used to fit the curves and calculate the stability constants.

The stability constants ( $\log K$ ) of the complexes with  $\text{Gd}^{3+}$  and  $\text{Zn}^{2+}$  ions follow the same order as their basicity, that is, (L3)<sup>4-</sup> > (L2)<sup>4-</sup> > (L1)<sup>4-</sup>. This result was expectable owing to the extra coordinating sites provided by the picolinate units with respect to acetates. However, the stability of  $[\text{Gd}(\text{L3})]^-$  remains lower than that of the octapa<sup>4-</sup> and cddadpa<sup>4-</sup> (cddadpa = 6,6'-[(cyclohexane-1,2-diylbis((carboxymethyl)azanediyl))bis(methylene)dipicolinic acid] analogues, suggesting that the cyclobutane ring imposes severe constraint and that this prevents the ligand from properly adapting to lanthanide coordination. Nevertheless, the  $\text{Gd}^{3+}$  complexes are

more stable for each of the three ligands than those of the endogenous  $\text{Zn}^{2+}$  cation. This aspect can be important to limit potential  $\text{Zn}^{2+}$  transmetalation of the  $\text{Gd}^{3+}$  complexes leading to  $\text{Gd}^{3+}$  release.

**Dissociation Kinetic Studies.** Kinetic inertness of metal complexes is a key parameter for their safe in vivo application. It is usually described by assessing the rate constants of the different pathways that can contribute to the overall dissociation. These involve spontaneous, acid- or metal-catalyzed processes (as depicted in Figure S4 in the Supporting Information), which are characterized by rate constants  $k_0$ ,  $k_1$ , and  $k_2$ , or  $k_3$ , respectively. While macrocyclic chelates are typically endowed with higher kinetic inertness, with rigidified open-chain ligands such as cddadpa<sup>6</sup> or HYD<sup>9b</sup> (Chart 1), kinetic inertness comparable to that of macrocyclic  $\text{Gd}^{3+}$  complexes could be achieved.

The kinetic inertness of  $[\text{Gd}(\text{L2})]^-$  was investigated by monitoring the exchange reaction with  $\text{Cu}^{2+}$ , which is a physiologically relevant metal ion with high efficiency to promote transmetalation of  $\text{Gd}^{3+}$  complexes in general. The transmetalation was followed by UV–vis spectrophotometry in the pH range of 3.5–4.9 at three different  $\text{Cu}^{2+}$  concentrations, corresponding to 20-, 30-, and 40-fold excess of the exchanging metal ion (Figure S5 in the Supporting Information). Unfortunately, for  $[\text{Gd}(\text{L3})]^-$  even at pH 6.1, the dissociation was too fast to be followed by conventional UV–vis spectroscopy or relaxometry, thus preventing a quantitative study. On the one hand, indeed, at pH 6.1 full dissociation was observed at 1 min following the mixing of the  $[\text{Gd}(\text{L3})]^-$  complex and 20 equiv of  $\text{Cu}^{2+}$ . On the other hand,  $[\text{Gd}(\text{L1})]^-$  was not studied in view of its lower stability. For  $[\text{Gd}(\text{L2})]^-$ , the pseudo-first-order rate constants,  $k_{\text{obs}}$ , as a function of the pH and the  $\text{Cu}^{2+}$  ion concentration, are shown in Figure 1.

The dissociation is independent of  $\text{Cu}^{2+}$  concentration, while it is strongly accelerated with decreasing pH, indicating that spontaneous and acid-catalyzed processes are responsible for the dissociation. This is in contrast to the dissociation of  $[\text{Gd}(\text{DTPA})]^{2-}$  (Chart 1) and some related open-chain



complexes, where metal-assisted pathways also represent a significant contribution.<sup>2a</sup>

The proton concentration dependence of the  $k_{\text{obs}}$  values could be fitted to eq 1, resulting in rate constants  $k_0$ ,  $k_1$ , and  $k_2$ , corresponding to the spontaneous dissociation ( $k_0$ ) and to the proton-catalyzed dissociation of the nonprotonated ( $k_1$ ) and the monoprotonated complex ( $k_2$ ). These rate constants are shown and compared to those of some related complexes in Table 2.

$$k_{\text{obs}} = k_0 + k_1[\text{H}^+] + k_2[\text{H}^+]^2 \quad (1)$$

The  $k_1 = 0.49 \text{ M}^{-1} \text{ s}^{-1}$  value for  $[\text{Gd}(\text{L2})]^-$  is similar to  $k_1$  for the clinically approved MRI agent  $[\text{Gd}(\text{DTPA})]^{2-}$ <sup>2a</sup> and the pyridine derivatives  $\text{GdPY}^{15}$  and  $\text{GdHYD}^{9b}$ , while it is 1 order of magnitude higher than that for the cyclohexane-derivative  $[\text{Gd}(\text{cddadpa})]^-$ .<sup>6</sup> The constant  $k_2$  is much lower than for  $[\text{Gd}(\text{DTPA})]^{2-}$ , whereas for  $[\text{Gd}(\text{cddadpa})]^-$ , this dissociation pathway was not important at all. When comparing to the pyridine derivatives  $\text{GdPY}$  and  $\text{GdHYD}$ ,  $[\text{Gd}(\text{L2})]^-$  has similar  $k_1$  but much higher  $k_2$ . Overall, the major difference between  $[\text{Gd}(\text{L2})]^-$  and all the other Gd complexes listed in Table 2 is in the rate constant characterizing the spontaneous dissociation,  $k_0$ . For  $[\text{Gd}(\text{L2})]^-$ ,  $k_0 = 3 \times 10^{-4} \text{ s}^{-1}$  is higher than the close-to-zero values reported for the other complexes, where  $k_0$  could be most often neglected in the analysis of the  $k_{\text{obs}}$  rate constants.

The dissociation half-life  $t_{1/2}$  was calculated using the available rate constants for physiological conditions (pH 7.4 and  $1 \mu\text{M}$   $\text{Cu}^{2+}$  concentration). Among the complexes with a rigidified ligand skeleton containing a pyridine ( $\text{GdPY}$ ,  $\text{GdHYD}$ ), a cyclohexane ( $\text{Gdcddadpa}$ ), or a cyclobutane ( $[\text{Gd}(\text{L2})]^-$ ) in the ligand backbone,  $[\text{Gd}(\text{L2})]^-$  has the shortest  $t_{1/2}$  and, thus, the lowest kinetic inertness. This is a direct consequence of the importance of the spontaneous dissociation pathway ( $k_0$ ) probably induced by the presence of the cyclobutane ring, while not present at all for the three other complexes ( $\text{GdPY}$ ,  $\text{GdHYD}$ , and  $\text{Gdcddadpa}$ ) with a rigidified backbone. At pH 7.4, this spontaneous pathway represents 100% of the overall dissociation, and even at pH 4, the spontaneous pathway is responsible for 80% of the overall rate. The importance of spontaneous dissociation is very unusual in general for lanthanide poly(aminocarboxylate) complexes. This represents an unexpected effect of further increasing the steric constraint in the ligand structure with respect to cyclohexane or pyridine derivatives. In addition, the picolinate function also likely contributes to reduce kinetic inertness, though at physiological pH this effect has no consequence for  $[\text{Gd}(\text{L2})]^-$ . Such an influence of the picolinate was previously reported for  $[\text{Gd}(\text{octapa})]^-$  as compared to  $[\text{Gd}(\text{edta})]^-$  ( $t_{1/2} = 0.15$  vs 55 h, respectively; pH 7.4 and  $1 \mu\text{M}$   $\text{Cu}^{2+}$ ). To explain this difference between  $[\text{Gd}(\text{octapa})]^-$  and  $[\text{Gd}(\text{edta})]^-$ , two factors have been evoked: (a) picolates increase the rate of the metal-ion-catalyzed dissociation pathway,<sup>2b</sup> as a result of their higher denticity, which favors the formation of the key dinuclear intermediate,  $\text{GdLCu}$ , in Cu-assisted dissociation; (b) the protonated picolinate complex has a significant kinetic activity in the decomplexation. For  $[\text{Gd}(\text{L2})]^-$ , we could not detect the metal-assisted pathway, but the high kinetic activity of the protonated complex at lower pH is an important factor, as it is evidenced by the high value of  $k_2$  (again, this has no effect at pH 7.4). For the bis(picolinate) derivative  $[\text{Gd}(\text{L3})]^-$  complex, it was impossible to derive dissociation rate constants and analyze the

contribution of the individual pathways and estimate the half-life for physiological conditions. One can simply conclude that, in this case, the addition of a second picolinate function is detrimental for the kinetic inertness (as experimentally assessed at pH 6 and 4). We note that a decrease in kinetic inertness upon increasing the ligand denticity has been already reported for linear  $\text{Mn}^{2+}$  complexes.<sup>16</sup> In general, such a situation can occur when the additional donor atoms of the ligand (i) contribute to more efficient proton-assisted dissociated pathways, since they provide more protonation sites and/or (ii) allow for the formation of dinuclear species, which would not be possible without those donor atoms.

**Luminescence Studies to Assess Hydration Numbers and Anion Binding.** Inner-sphere proton relaxivity is linearly proportional to the number  $q$  of inner-sphere water molecules in the  $\text{Gd}^{3+}$  complexes.<sup>2</sup> Hydration numbers have been determined on the corresponding  $[\text{Eu}(\text{L1})]^-$ ,  $[\text{Eu}(\text{L2})]^-$ , and  $[\text{Eu}(\text{L3})]^-$  analogues, by measuring luminescence lifetimes in  $\text{H}_2\text{O}$  and  $\text{D}_2\text{O}$  solutions (Table 3, see Figure S7 for

**Table 3. Luminescence Decay Lifetimes ( $\tau$ ) and Calculated Hydration Numbers ( $q$ )**

complex <sup>a</sup>	$\tau_{\text{H}_2\text{O}}$ (ms)	$\tau_{\text{D}_2\text{O}}$ (ms)	$q^b$	$q^c$
$[\text{Eu}(\text{L1})]^-$	0.241	0.760	3.1	2.8
$[\text{Eu}(\text{L2})]^-$	0.405	2.16	2.1	1.9
$[\text{Eu}(\text{L3})]^-$	0.544	1.984	1.3	1.1

<sup>a</sup>Concentrations of complexes were 0.2 mM, 0.1 M Hepes buffer, pH, pD = 7, 25 °C. <sup>b</sup>The  $q$  values were obtained from eq 2 with  $A = 1.2$  and  $B = 0.25$ . <sup>c</sup>eq 2 with  $A = 1.11$  and  $B = 0.31$ .

the absorption spectra of L2 and  $[\text{Eu}(\text{L2})]^-$ , as well as the emission and excitation spectra of  $[\text{Eu}(\text{L2})]^-$  as an example).<sup>17,18</sup> All luminescence decay curves were mono-exponential (Figure S8). The following empiric equation (eq 2) is used to calculate  $q$  from the differences of luminescence decay lifetime in  $\text{H}_2\text{O}$  and  $\text{D}_2\text{O}$ ,  $\tau_{\text{H}_2\text{O}}$  and  $\tau_{\text{D}_2\text{O}}$ , ( $A = 1.2$  and  $B = 0.25$ <sup>19</sup> or  $A = 1.11$  and  $B = 0.31$ <sup>20</sup>).

$$q = A \left( \frac{1}{\tau_{\text{H}_2\text{O}}} - \frac{1}{\tau_{\text{D}_2\text{O}}} - B \right) \quad (2)$$

As expected on the basis of ligand denticity, the hydration numbers ( $q$ ) are 3, 2, and 1 for  $[\text{Eu}(\text{L1})]^-$ ,  $[\text{Eu}(\text{L2})]^-$ , and  $[\text{Eu}(\text{L3})]^-$ , respectively. Figure 2 shows the structures for the three hydrated  $\text{Gd}^{3+}$  complexes.

Lanthanide chelates containing more than one inner-sphere water molecule are often prone to ternary complex formation with endogenous anions, such as carbonate, phosphate, or citrate.<sup>21–23</sup> These anions replace the hydration water molecules and lead to a drastic relaxivity decrease of the  $\text{Gd}^{3+}$  complexes.<sup>24</sup> It has been previously shown that, for bis(hydrated) complexes, the inner-sphere structure and the respective position of the two inner-sphere water molecules are primordial to induce or to prevent ternary complex formation.<sup>25</sup> While  $\text{GdDO3A}$  easily undergoes ternary complex formation, several bis(hydrated), linear complexes, such as  $\text{GdHYD}$ ,  $\text{GdPY}$ , etc., proved to be resistant.<sup>26</sup>

The formation of ternary complexes between  $[\text{Gd}(\text{L1})]^-$ ,  $[\text{Gd}(\text{L2})]^-$ , or  $[\text{Gd}(\text{L3})]^-$  and carbonate and phosphate, two abundant physiological anions (22–29 and 1.12–1.45 mM concentrations, respectively, in the blood), was studied by measuring the luminescence lifetime of their related  $\text{Eu}^{3+}$

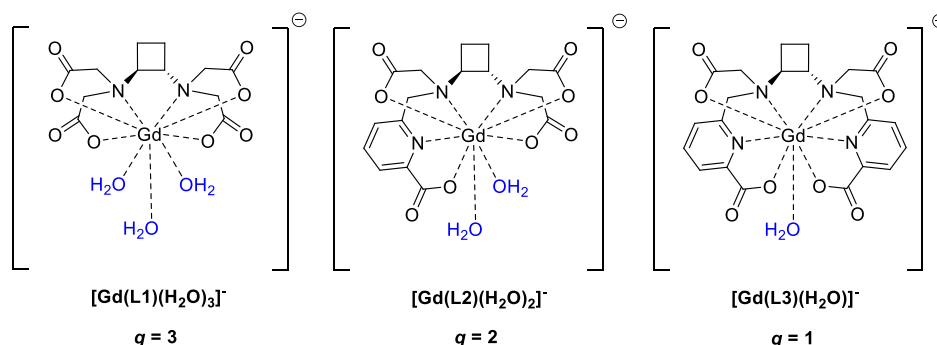


**Figure 2.** Structures and  $q$  values for  $[\text{Gd}(\text{L1})(\text{H}_2\text{O})_3]^-$ ,  $[\text{Gd}(\text{L2})(\text{H}_2\text{O})_2]^-$ , and  $[\text{Gd}(\text{L3})(\text{H}_2\text{O})]^-$  complexes. Charges are omitted for clarity.

complexes in  $\text{H}_2\text{O}$  and  $\text{D}_2\text{O}$ . These two anions can interact differently with lanthanide complexes; phosphate has been demonstrated to bind in a monodentate way, while carbonate typically binds in a bidentate manner. The luminescence emission decays of the  $\text{Eu}^{3+}$  complexes were recorded in  $\text{H}_2\text{O}$  and  $\text{D}_2\text{O}$ , in the presence of 10 and 50 equiv of carbonate and phosphate (50 equiv are above the physiological concentrations of this anion in human plasma), and the hydration numbers were calculated according to eq 2 (Table 4).

**Table 4.**  $q$  Values for  $[\text{Eu}(\text{L1})]^-$ ,  $[\text{Eu}(\text{L2})]^-$ , and  $[\text{Eu}(\text{L3})]^-$  in the Absence or in the Presence of 10 and 50 Equivalents of Phosphate and Carbonate, Respectively<sup>a</sup>

complex	anion free $[\text{EuL}]^-$	$q^a$			
		phosphate		carbonate	
		10 eq	50 eq	10 eq	50 eq
$[\text{Eu}(\text{L1})]^-$	3.1	2.4	2.4	2.0	2.1
$[\text{Eu}(\text{L2})]^-$	2.1	2.2	2.1	2.1	2.0
$[\text{Eu}(\text{L3})]^-$	1.3	1.3	1.2	1.3	1.3

<sup>a</sup>The  $q$  values were obtained from eq 2 with  $A = 1.2$  and  $B = 0.25$ ; 0.2 mM EuL, 0.1 M Hepes buffer, pH, pD = 7.4, 25 °C.

The  $q$  values of  $[\text{Eu}(\text{L2})]^-$  and  $[\text{Eu}(\text{L3})]^-$  did not decrease with the addition of 10 and 50 equiv of phosphate or carbonate, excluding the formation of ternary  $\text{Eu}^{3+}$  complexes with these anions. In contrast, the number of water molecules in  $[\text{Eu}(\text{L1})]^-$  complex decreased by 22% when phosphate was added and up to 35% in the presence of carbonate (Figure S6 in the Supporting Information). These results suggest that stability follows the trend  $[\text{Eu}(\text{L3})]^- \approx [\text{Eu}(\text{L2})]^- \gg [\text{Eu}(\text{L1})]^-$ . Moreover, this tendency is confirmed by the time dependence of the luminescence intensity shown in Figure S8.

**DFT Calculations.** DFT calculations were performed to gain insight into the relation between molecular structure and the thermodynamic and kinetic properties of  $[\text{Gd}(\text{L2})]^-$  and  $[\text{Gd}(\text{L3})]^-$  complexes. On the grounds of previous studies, our calculations included two explicit second-sphere water molecules hydrogen-bonded to each of the coordinated water molecules, while bulk solvent effects were introduced by using a polarized continuum model (PCM). The use of mixed cluster-PCM models is important to achieve a better description of the solution structures of  $\text{Gd}^{3+}$  complexes with polyamino polycarboxylate ligands, in particular, regarding the Gd–O<sub>water</sub> distances and the spin density at the O nuclei of the water molecule.<sup>27</sup> For the sake of comparison, we also performed DFT calculations on the  $[\text{Gd}(\text{cddadpa})(\text{H}_2\text{O})]^-$

and octadentate coordination of the ligands to the metal ion, as expected. Our calculations predict rather long Gd–N distances involving the amine nitrogen atoms of the ligands, an effect that is more striking in the case of the complex of  $(\text{L3})^{4-}$  (Figure 3, Table 5). These Gd–N distances are considerably longer than those calculated for the  $[\text{Gd}(\text{cddadpa})(\text{H}_2\text{O})]^-$  complex (2.81 and 2.75 Å), reflecting a better accommodation of the  $\text{Gd}^{3+}$  ion in the cavity of the latter. We also notice that the stability of the  $[\text{Lu}(\text{L3})(\text{H}_2\text{O})]^-$  complex is 1 order of magnitude lower than that of the  $\text{Gd}^{3+}$  analogue (Table 1). This can be attributed to the larger bite angle imposed by the cyclobutanediimine unit, as estimated from the N–Gd–N angles of 69.1 and 65.7° calculated for the structurally related  $[\text{Gd}(\text{L3})(\text{H}_2\text{O})]^-$  and  $[\text{Gd}(\text{cddadpa})(\text{H}_2\text{O})]^-$  complexes.

The analysis of the electrostatic potential calculated with DFT on isodensity surfaces defined by a 0.001 a.u. contour of the electron density<sup>28</sup> provides additional valuable information to rationalize the different dissociation kinetic profiles of  $[\text{Gd}(\text{L2})(\text{H}_2\text{O})_2]^-$  and  $[\text{Gd}(\text{L3})(\text{H}_2\text{O})]^-$ . As for other  $\text{Ln}^{3+}$

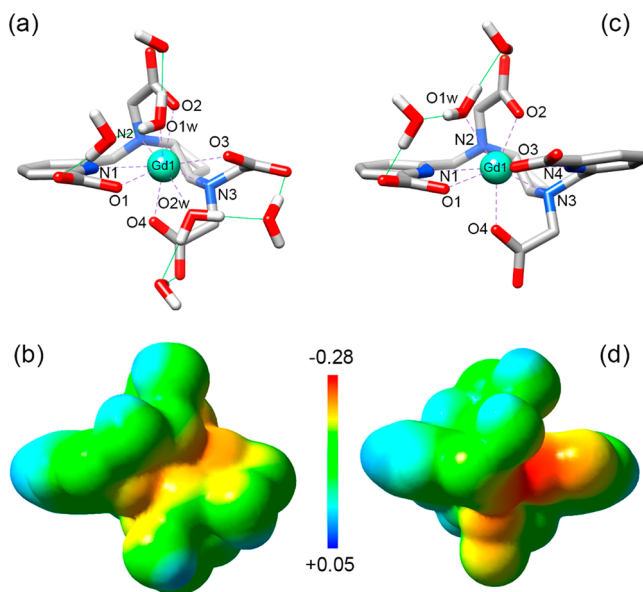


**Figure 3.** Calculated structure (a) and (c), and electrostatic potential (b) and (d) of  $[\text{Gd}(\text{L2})(\text{H}_2\text{O})_2]^-$  and  $[\text{Gd}(\text{L3})(\text{H}_2\text{O})]^-$ , respectively. Electrostatic potentials (hartree) are mapped on the molecular surfaces defined by the 0.001 electrons-bohr<sup>-3</sup> contour of the electronic densities.

and octadentate coordination of the ligands to the metal ion, as expected. Our calculations predict rather long Gd–N distances involving the amine nitrogen atoms of the ligands, an effect that is more striking in the case of the complex of  $(\text{L3})^{4-}$  (Figure 3, Table 5). These Gd–N distances are considerably longer than those calculated for the  $[\text{Gd}(\text{cddadpa})(\text{H}_2\text{O})]^-$  complex (2.81 and 2.75 Å), reflecting a better accommodation of the  $\text{Gd}^{3+}$  ion in the cavity of the latter. We also notice that the stability of the  $[\text{Lu}(\text{L3})(\text{H}_2\text{O})]^-$  complex is 1 order of magnitude lower than that of the  $\text{Gd}^{3+}$  analogue (Table 1). This can be attributed to the larger bite angle imposed by the cyclobutanediimine unit, as estimated from the N–Gd–N angles of 69.1 and 65.7° calculated for the structurally related  $[\text{Gd}(\text{L3})(\text{H}_2\text{O})]^-$  and  $[\text{Gd}(\text{cddadpa})(\text{H}_2\text{O})]^-$  complexes.

The analysis of the electrostatic potential calculated with DFT on isodensity surfaces defined by a 0.001 a.u. contour of the electron density<sup>28</sup> provides additional valuable information to rationalize the different dissociation kinetic profiles of  $[\text{Gd}(\text{L2})(\text{H}_2\text{O})_2]^-$  and  $[\text{Gd}(\text{L3})(\text{H}_2\text{O})]^-$ . As for other  $\text{Ln}^{3+}$

**Table 5. Bond Distances of the Gd<sup>3+</sup> Coordination Environments (Å) Obtained with DFT Calculations**

	GdL2	GdL3	Gdcddadpa
Gd1–N1	2.744	2.785	2.599
Gd1–N2	2.917	3.034	2.748
Gd1–N3	2.789	2.875	2.805
Gd1–N4		2.701	2.646
Gd1–O1	2.423	2.419	2.446
Gd1–O2	2.389	2.390	2.394
Gd1–O3	2.422	2.392	2.450
Gd1–O4	2.417	2.361	2.381
Gd1–O1w	2.482	2.519	2.570
Gd1–O2w	2.474		

poly(aminocarboxylate) complexes,<sup>29</sup> the surfaces of the complexes present a hydrophilic region containing the carboxylate groups and coordinated water molecules, and a hydrophobic side containing the pyridyl rings and cyclobutane rings. In the [Gd(L3)(H<sub>2</sub>O)]<sup>−</sup>·2H<sub>2</sub>O complex, three coordinated carboxylate oxygen atoms are placed in the same region of the complex surface, rendering a more negative electrostatic potential than for the [Gd(L2)(H<sub>2</sub>O)]<sup>−</sup> complex (O1, O3, and O4, Figure 3). This result is in agreement with the higher protonation constant determined with potentiometric measurements for [Gd(L3)(H<sub>2</sub>O)]<sup>−</sup> ( $K_{\text{GdHL}} = 3.28$ ) compared with [Gd(L2)(H<sub>2</sub>O)<sub>2</sub>]<sup>−</sup> ( $\log K_{\text{GdHL}} = 2.36$ ). Thus, the much faster complex dissociation of [Gd(L3)(H<sub>2</sub>O)]<sup>−</sup> is likely related to the tendency of this complex to protonate, which together with the long Gd–N distances provides a low-energy path for complex dissociation. Similarly, the lack of contribution of a metal-assisted pathway to the dissociation of [Gd(L2)(H<sub>2</sub>O)<sub>2</sub>]<sup>−</sup> must be related to its rather open structure, which yields a molecular surface with lower negative electrostatic potential and thus a lower tendency to form the key dinuclear intermediate.

The two coordinated water molecules in [Gd(L2)(H<sub>2</sub>O)<sub>2</sub>]<sup>−</sup>·4H<sub>2</sub>O present relatively similar calculated Gd–O<sub>water</sub> distances (2.482 and 2.474 Å, Figure 3). The ligand wraps around the Gd<sup>3+</sup> ion resulting in a set of five donor atoms of the ligand arranged in a relatively planar fashion (O1, O3, N1, N2, and N3), with one of the carboxylate ligands containing O2 and O4 coordinating above and below this plane, respectively. The two coordinated water molecules approach the metal ion from different sides of the mean plane. As a result, the oxygen atoms of these water molecules define a rather open O–Gd–O angle of 88.4°.

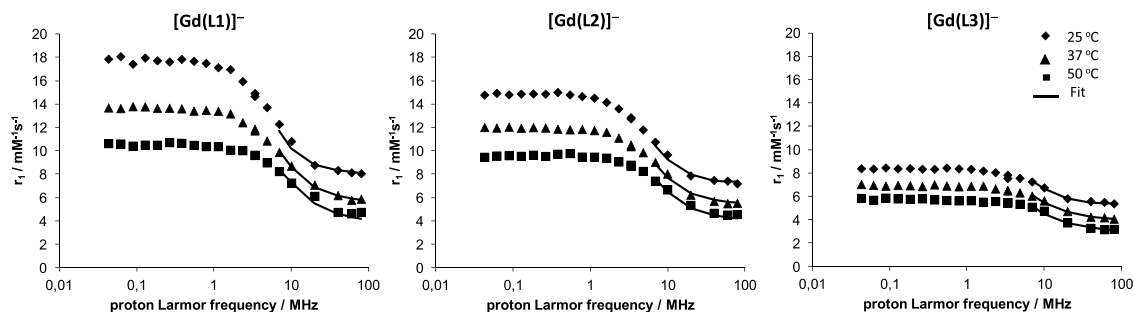
This orientation of the inner-sphere water molecules, together with the negative charge of the complex, is likely responsible for the lack of binding of carbonate and phosphate described above.

**NMRD and <sup>17</sup>O NMR Studies.** According to the Solomon–Bloembergen–Morgan theory of paramagnetic relaxation, the relaxivity is related to a number of microscopic parameters of the paramagnetic chelate, which involve the number of hydration water molecules, the water exchange rate, the rotational dynamics of the complex, and its electron spin relaxation. To describe these parameters, nuclear magnetic relaxation dispersion (NMRD) profiles were recorded for [Gd(L1)]<sup>−</sup>, [Gd(L2)]<sup>−</sup>, and [Gd(L3)]<sup>−</sup> complexes in the field range of 0.01–80 MHz at 25, 37, and 50 °C. The NMRD curves reflect the magnetic field dependency of the proton relaxivity and are helpful to distinguish between different relaxation mechanisms. The profiles of all three complexes (Figure 4) have the shape typical of low molecular weight chelates with a single dispersion between 1 and 10 MHz. The relaxivity values decrease with increasing temperature, which is consistent with fast rotation of the complex that limits the relaxivity. The relaxivity values measured at 20 MHz and 25 °C (Table 6) are in coherence with the size and the hydration number of the chelates.

Compared with other complexes described in the literature, we can observe that the relaxivity of bis(hydrated) [Gd(L2)]<sup>−</sup> is very similar to that of [Gd(CyPic3A)]<sup>−</sup> under the same conditions; an identical trend is observed comparing monohydrated complexes [Gd(L3)]<sup>−</sup> and [Gd(cddadpa)]<sup>−</sup>. Both [Gd(L2)]<sup>−</sup> and [Gd(L3)]<sup>−</sup> present higher values for relaxivity, almost twice that of [Gd(DTPA)]<sup>−</sup>, for instance.

The relaxivities were also measured in the presence of physiological concentration (0.6 mM) of human serum albumin (HSA) at 20 and 60 MHz, 37 °C. These values are 30–40% higher than those recorded in the absence of HSA (see Supporting Information), indicating a weak binding to the protein.

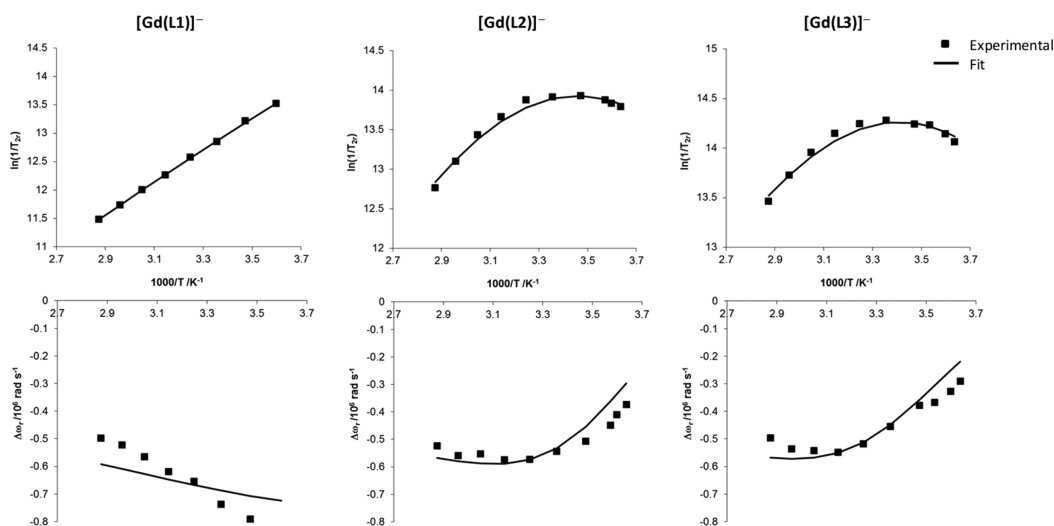
The NMRD studies have been complemented by variable-temperature <sup>17</sup>O transverse relaxation rate and chemical shift measurements, which allow, respectively, direct assessment of the water exchange rate and estimation of the hydration number. Figure 5 shows the variable-temperature, reduced transverse <sup>17</sup>O relaxation times and chemical shifts for the three gadolinium complexes recorded at 54.2 MHz (9.4 T). The luminescence lifetime measurements indicated 3, 2, and 1 inner-sphere water molecules for [Eu(L1)]<sup>−</sup>, [Eu(L2)]<sup>−</sup>, and [Eu(L3)]<sup>−</sup>, respectively, and the <sup>17</sup>O chemical shifts measured on the Gd<sup>3+</sup> analogues are in accordance with this. Indeed, the



**Figure 4.** NMRD profiles of 1.88 mM [Gd(L1)]<sup>−</sup>, 1.91 mM [Gd(L2)]<sup>−</sup>, and 2.13 mM [Gd(L3)]<sup>−</sup> in water at pH = 7 and temperatures of 25, 37, and 50 °C. Curves represent the simultaneous fit as described in the text.

**Table 6.** Relaxivity Values,  $r_1$  ( $\text{mM}^{-1} \text{s}^{-1}$ ), for  $[\text{Gd}(\text{L1})]^-$ ,  $[\text{Gd}(\text{L2})]^-$ , and  $[\text{Gd}(\text{L3})]^-$ , and Related  $\text{Gd}^{3+}$  Complexes from the Literature, at  $25^\circ \text{C}$ 

	$[\text{Gd}(\text{L1})]^-$	$[\text{Gd}(\text{L2})]^-$	$[\text{Gd}(\text{L3})]^-$	$[\text{Gd}(\text{CyPic3A})]^-$ <sup>9a</sup>	$[\text{Gd}(\text{cddadpa})]^-$ <sup>6</sup>	$[\text{Gd}(\text{DTPA})]^-$ <sup>30</sup>
$r_1^a$	8.8	7.9	5.8	8.3	5.6	4.3
$r_1^b$	8.1	7.4	5.5	7.9		
$q$	3	2	1.2	2	1	1

<sup>a</sup>20 MHz (0.47 T). <sup>b</sup>60 MHz (1.41 T).**Figure 5.** Reduced transverse  $^{17}\text{O}$  NMR relaxation rates (top) and  $^{17}\text{O}$  NMR chemical shifts (bottom) of the following aqueous solutions:  $15.3 \text{ mmol kg}^{-1}$   $[\text{Gd}(\text{L1})]^-$ ,  $14.5 \text{ mmol kg}^{-1}$   $[\text{Gd}(\text{L2})]^-$ , and  $6.46 \text{ mmol kg}^{-1}$   $[\text{Gd}(\text{L3})]^-$  at  $\text{pH} = 6.5$ . Curves represent the simultaneous fit.**Table 7.** Relaxivities (20 MHz,  $25^\circ \text{C}$ ) and Parameters Obtained from the Simultaneous Fitting of  $^{17}\text{O}$  NMR and NMRD Data for  $[\text{Gd}(\text{L1})]^-$ ,  $[\text{Gd}(\text{L2})]^-$ , and  $[\text{Gd}(\text{L3})]^-$  and Literature Values for Related Complexes  $[\text{Gd}(\text{HYD})]^-$ ,<sup>9b</sup>  $[\text{Gd}(\text{CyPic3A})]^-$ ,<sup>9a</sup> and  $[\text{Gd}(\text{DTPA})]^-$ <sup>2–30</sup>

	$[\text{Gd}(\text{L1})]^-$	$[\text{Gd}(\text{L2})]^-$	$[\text{Gd}(\text{L3})]^-$	$[\text{Gd}(\text{HYD})]^-$ <sup>9b</sup>	$[\text{Gd}(\text{CyPic3A})]^-$ <sup>9a</sup>	$[\text{Gd}(\text{DTPA})]^-$ <sup>2–30</sup>
$k_{\text{ex}}^{298}$ ( $10^6 \text{ s}^{-1}$ )	$127 \pm 15$	$10.0 \pm 2.3$	$8.1 \pm 0.5$	7.8	44	3.3
$\Delta H^\ddagger$ ( $\text{kJ mol}^{-1}$ )	$21.7 \pm 3.6$	$36.1 \pm 1.6$	$27.6 \pm 1.7$	43.5	29.1	51.6
$\Delta S^\ddagger$ ( $\text{J mol}^{-1} \text{K}^{-1}$ )	$-17 \pm 7$	$+10 \pm 4$	$-1 \pm 5$	+33		+53
$\tau_{\text{RH}}^{298}$ (ps)	$66 \pm 2$	$92 \pm 3$	$119 \pm 2$	92.6		58
$\tau_{\text{V}}^{298}$ (ps)	$15 \pm 2$	$2.6 \pm 0.5$	$3.8 \pm 0.2$	2.1		
$E_{\text{R}}$ ( $\text{kJ mol}^{-1}$ )	$23.8 \pm 0.6$	$20.1 \pm 1.3$	$20.5 \pm 0.7$	21.0		17.3
$A/\hbar$ ( $10^6 \text{ rad s}^{-1}$ )	$-3.1 \pm 0.2$	$-3.0 \pm 0.4$	$-3.1 \pm 0.3$	-4.0		-3.8
$\Delta^2$ ( $10^{20} \text{ s}^{-2}$ )	$0.44 \pm 0.07$	$0.46 \pm 0.13$	$0.40 \pm 0.02$	0.55		
$q$	3	2	1	2	2	1

scalar coupling constants fitted for the three chelates are approximately  $A/\hbar \approx -(3.0\text{--}3.1) \times 10^6 \text{ rad s}^{-1}$ , at the lower limit of typical values reported for  $\text{Gd}^{3+}$  complexes. DFT calculations performed on the  $[\text{Gd}(\text{L2})(\text{H}_2\text{O})_2]^- \cdot 4\text{H}_2\text{O}$  and  $[\text{Gd}(\text{L3})(\text{H}_2\text{O})]^- \cdot 2\text{H}_2\text{O}$  systems (see computational details below) provide  $A/\hbar$  values of  $-3.8 \times 10^6$  and  $-2.7 \times 10^6 \text{ rad s}^{-1}$ , in reasonable agreement with the experimental data. This also confirms the hydration number of the complexes determined by luminescence lifetime measurements. The  $A/\hbar$  determined for  $[\text{Gd}(\text{L3})(\text{H}_2\text{O})]^- \cdot 2\text{H}_2\text{O}$  is somewhat higher than those determined for  $[\text{Gd}(\text{octa})(\text{H}_2\text{O})]^-$  using  $^{17}\text{O}$  NMR measurements ( $A/\hbar = -2.3 \times 10^6 \text{ rad s}^{-1}$ )<sup>2i</sup> and DFT calculations ( $A/\hbar = -2.5 \times 10^6 \text{ rad s}^{-1}$ ).<sup>31</sup> The relatively low values of  $A/\hbar$  determined for these series of complexes might be related to a rather efficient delocalization of the spin density through the aromatic picolinate units.

The difference in the temperature dependence of the transverse  $^{17}\text{O}$  relaxation rates shows that the three complexes

have different water exchange rates. While the tris(hydrated)  $[\text{Gd}(\text{L1})]^-$  is in the fast exchange regime in the entire temperature range ( $1/T_{2r}$  increases with decreasing temperature),  $[\text{Gd}(\text{L2})]^-$  and  $[\text{Gd}(\text{L3})]^-$  are in the fast exchange regime at high temperatures and in an intermediate range at lower temperatures. The temperature dependency of the chemical shifts follows the same trend. The transverse relaxation rate of the coordinated water oxygen,  $1/T_{2m}$ , determines  $1/T_{2r}$  in the fast exchange region. In turn,  $1/T_{2m}$  is influenced by the following parameters: the water exchange rate  $k_{\text{ex}}$ , the longitudinal electronic relaxation rate  $1/T_{1e}$ , and the scalar coupling constant  $A/\hbar$ .

The reduced transverse  $^{17}\text{O}$  relaxation rates and chemical shifts were fitted together with the NMRD profiles according to the SBM theory. The following parameters were calculated: the water exchange rate  $k_{\text{ex}}^{298}$ , the activation enthalpy  $\Delta H^\ddagger$  and entropy  $\Delta S^\ddagger$ , the scalar coupling constant  $A/\hbar$ , the rotational correlation time  $\tau_{\text{RH}}$ , its activation energy  $E_{\text{R}}$ , and the



parameters referring to electron spin relaxation, namely,  $\Delta^2$  and  $\tau_v^{298}$ . The distances between the  $Gd^{3+}$  ion and the protons in the inner and outer coordination sphere were fixed to typical values,  $r_{GdH} = 3.1$  Å and  $a_{GdH} = 3.6$  Å, respectively, and the diffusion coefficient and its activation energy were fixed to  $D_{GdH}^{298} = 26 \times 10^{-10} \text{ m}^2 \text{ s}^{-1}$  and  $E_{DGdH} = 20 \text{ kJ mol}^{-1}$ . Reliable information on dynamic processes, like water exchange and rotational correlation times for small complexes, can be obtained by application of the SBM approach to the analysis of the NMRD data at medium and high magnetic fields, provided that detailed information about electron spin relaxation is not required.<sup>32</sup> Consequently, only relaxivity values above 6 MHz were included in the fitting. The number of water molecules  $q$  directly coordinated to  $Gd^{3+}$  was fixed to 3, 2, and 1 for  $[Gd(L1)]^-$ ,  $[Gd(L2)]^-$ , and  $[Gd(L3)]^-$ , respectively.

The equations used are given in the Supporting Information, and the parameters obtained are shown in Table 7.

While there is a slight increase in the water exchange rate from  $[Gd(L3)]^-$  to  $[Gd(L2)]^-$  ( $k_{ex}^{298} = 8.1 \times 10^6$  and  $10.0 \times 10^6 \text{ s}^{-1}$ , respectively),  $[Gd(L1)]^-$  has 1 order of magnitude faster water exchange ( $k_{ex}^{298} = 127 \times 10^6 \text{ s}^{-1}$ ), which is only 6 times lower than that of the aqua ion  $[Gd(H_2O)_8]^{3+}$  ion ( $800 \times 10^6 \text{ s}^{-1}$ ). The reason for this very fast exchange is likely the high flexibility of the inner coordination sphere around the binding site of the three hydration water molecules, despite the rigid ligand structure. In addition, the negative value of the activation entropy points to an associatively activated mechanism for  $[Gd(L1)]^-$ , which means that the incoming water molecule has also a role in the rate-determining step. On the one hand, while only the determination of activation volumes via variable-pressure  $^{17}\text{O}$  NMR measurements would allow for a precise assessment of the water exchange mechanism, activation entropies also provide a hint.<sup>33</sup> On the other hand,  $[Gd(L2)]^-$  and  $[Gd(L3)]^-$  are characterized by an interchange or slightly dissociatively activated water exchange mechanism (the activation entropy is close to zero or has a small positive value), in contrast to the high positive  $\Delta S^\ddagger$  value for  $[Gd(DTPA)]^{2-}$ , clearly indicating a dissociative mechanism.

The calculated values of the rotational correlation time,  $\tau_{RH}^{298}$ , were 66, 92, and 119 ps, for  $[Gd(L1)]^-$ ,  $[Gd(L2)]^-$ , and  $[Gd(L3)]^-$ , respectively, in accordance with their increasing size. The small differences in the relaxivity of the three complexes can be related to the opposing effects of the decreasing hydration number and the increasing size, hence, rotational correlation time in the order of  $[GdL1]^-$ ,  $[Gd(L2)]^-$ , and  $[Gd(L3)]^-$ . The water exchange rate has no influence on relaxivity for such small complexes; their relaxivity is only limited by fast rotation.

## CONCLUSIONS

In this work, we have described efficient syntheses of three different ligands containing a rigid (1*S*,2*S*)-1,2-cyclobutanediamine spacer and a different number of acetate and picolinate groups. We have shown that this versatile spacer can be easily functionalized with different coordinating groups, providing a new structural entry for ligand design to coordination chemists. We expected that the rigid nature of the spacer could provide  $Gd^{3+}$  complexes with high kinetic inertness. Although detailed dissociation kinetic data could not be obtained for  $[Gd(L3)]^-$ , thermodynamic and luminescence studies as well as computational calculations suggest that the octadentate ligand (L3)<sup>4-</sup>

forms a stable, monohydrated complex with  $Gd^{3+}$ , which is very labile. In contrast, the complex with the heptadentate (L2)<sup>4-</sup> ligand presents a much higher kinetic inertness together with a rather high relaxivity associated with the presence of two coordinated water molecules. While the inertness of the complex is not good enough to conceive any in vivo application as an MRI contrast agent, this complex represents a rare case in which lowering ligand denticity causes a noticeable increase in kinetic inertness.<sup>34</sup> A structural analysis suggests that the large bite angle of the (1*S*,2*S*)-1,2-cyclobutanediamine spacer can make ligands based on this scaffold more suitable for the coordination of bulkier metal ions. Future work will expand the family of ligands presented here and will explore their coordination properties toward other metal ions with relevant biomedical applications.

## EXPERIMENTAL SECTION

**Tetra(*tert*-butyl) 2,2',2'',2'''-[[{(1*S*,2*S*)-cyclobutane-1,2-diyl]-bis(azanediyl)]tetraacetate (3).** To a solution of 2 (65.6 mg, 0.75 mmol), prepared according to ref 10, potassium iodide (480 mg, 2.89 mmol, 3.85 equiv), and diisopropylethylamine (1.08 mL, 6.2 mmol, 8.3 equiv) in dimethylformamide (DMF) (2 mL) was added *tert*-butyl bromoacetate (0.49 mL, 3.3 mmol, 4.4 equiv), and the reaction mixture was stirred at room temperature for 18 h under  $N_2$  atmosphere. Then, the solution was diluted with  $CH_2Cl_2$  (20 mL) and washed with saturated  $K_2CO_3$  ( $2 \times 5$  mL) and brine ( $1 \times 5$  mL). The organic layer was dried over  $MgSO_4$ , filtered, and evaporated under reduced pressure. Purification by column chromatography (1:3 ethyl acetate (EtOAc)/hexane) afforded 3 (288 mg, 0.53 mmol, 70% yield) as a yellow oil.  $[\alpha]_D^{20}$ : +8 ( $c = 1.0$ ,  $CH_3OH$ );  $^1H$  NMR (360 MHz,  $CDCl_3$ ):  $\delta$  1.44 (s, 28H,  $^tBu$ ,  $H_3$ ,  $H_4$ ), 1.79 (m, 2H,  $H_2'$ ,  $H_4'$ ), 3.32 (m, 2H,  $H_1$ ,  $H_2$ ), 3.41 (m, 1H,  $H_5$ ), 3.46 (m, 3H,  $H_5$ ), 3.49 (m, 3H,  $H_5$ ), 3.54 (m, 1H,  $H_5$ );  $^{13}C$  NMR (90 MHz,  $CDCl_3$ ):  $\delta$  20.3 ( $C_3$ ,  $C_4$ ), 28.1 ( $^tBu$ ), 52.9 ( $C_5$ ), 62.9 ( $C_1$ ,  $C_2$ ), 80.6 ( $C-^tBu$ ), 171.1 (CO). IR (ATR):  $\nu$  2978, 2931, 1729  $cm^{-1}$ ; HRMS (electrospray ionization (ESI))  $m/z$  calcd for  $C_{28}H_{51}N_2O_8$  [ $M + H$ ]<sup>+</sup>: 543.3640. Found: 543.3647.

**2,2',2'',2'''-[[{(1*S*,2*S*)-Cyclobutane-1,2-diyl]bis(azanediyl)]-tetraacetic acid ( $H_4cbdta$ ,  $H_4(L1)$ ).** A solution of compound 3 (180 mg, 0.33 mmol) in 4 M HCl in dioxane (12 mL) was stirred at room temperature for 18 h. Then, the solvent was evaporated under reduced pressure, and a small amount of water (2 mL) was added, and the mixture was evaporated to dryness. This process was repeated once with the addition of water and twice with an addition of diethyl ether (2 mL) to afford the desired ligand (110 mg, 0.25 mmol, 77% yield) as a yellow solid.  $^1H$  NMR (600 MHz,  $D_2O$ ):  $\delta$  1.67 (m, 2H,  $H_3$ ,  $H_4$ ), 1.97 (m, 2H,  $H_3$ ,  $H_4$ ), 3.88 (m, 8H,  $H_5$ ), 3.94 (m, 2H,  $H_1$ ,  $H_2$ );  $^{13}C$  NMR (150 MHz,  $D_2O$ ):  $\delta$  18.1 ( $C_3$ ,  $C_4$ ), 52.5 ( $C_5$ ), 61.7 ( $C_1$ ,  $C_2$ ), 171.2 (CO). HRMS(ESI)  $m/z$  calcd for  $C_{12}H_{18}N_2O_8Na$  [ $M + Na$ ]<sup>+</sup>: 341.0961. Found: 341.0962.

**Methyl 6-[[{(1*S*,2*S*)-cyclobutane-1,2-diyl]bis[(2-*tert*-butoxycarbonyl)azanediyl]] (methylene)]picolinate (6).** Aldehyde 5 (0.124 g, 0.75 mmol, 1 equiv), prepared according to ref 2b, was added to a solution of 4<sup>10</sup> (140 mg, 0.75 mmol) in  $CH_3OH$  (5 mL), and the reaction mixture was stirred at room temperature for 2.5 h. Small aliquots of this reaction were removed and concentrated to dryness for NMR analysis to confirm full Schiff base formation. Then, the reaction was diluted with  $CH_3OH$  (5 mL) and cooled to 0 °C, and then  $NaBH_4$  (31 mg, 0.81 mmol) was added. After it was stirred for 2 h at 0 °C, the reaction was quenched with saturated (satd)  $NaHCO_3$  and extracted with  $CH_2Cl_2$ . The organic layer was dried over  $MgSO_4$ , filtered, and evaporated under reduced pressure to afford 6 (218 mg, 0.65 mmol, 87% yield) as a yellow oil.  $[\alpha]_D^{20}$ : +5 ( $c = 1.0$ ,  $CH_3OH$ );  $^1H$  NMR (400 MHz,  $CDCl_3$ ):  $\delta$  1.42 (s, 11H,  $^tBu$ ,  $H_3$ ,  $H_4$ ), 1.95 (m, 1H), 2.12 (m, 1H), 2.87 (br s, 2H, NH), 3.15 (m, 1H), 3.79 (m, 1H), 3.98 (s, 3H, Me), 4.01 (m, 2H,  $H_5$ ), 7.55 (m, 1H), 7.78 (m, 1H), 7.97 (m, 1H);  $^{13}C$  NMR (90 MHz,  $CDCl_3$ ):  $\delta$  23.3, 23.5, 28.3, 52.2, 52.8, 61.5, 64.5, 77.2, 123.7, 125.7, 137.6, 146.9,

154.9, 160.3, 165.5; IR (attenuated total reflectance (ATR)):  $\nu$  3117, 2975, 1687  $\text{cm}^{-1}$ ; HRMS(ESI)  $m/z$  calcd for  $\text{C}_{17}\text{H}_{25}\text{N}_3\text{O}_4\text{Na}$  [ $\text{M} + \text{Na}$ ] $^+$ : 358.1737. Found: 358.1724.

**Methyl 6-[[[(1S,2S)-cyclobutane-1,2-diyltris(2-*tert*-butoxy-2-oxoethyl)azanediyl]](methylene)] picolinate (7).** Diamine **6** (218 mg, 0.65 mmol) was dissolved in  $\text{CH}_2\text{Cl}_2$  (5 mL). Then, a solution of 1 M HCl in EtOAc (11.25 mL, 11.25 mmol, 15 equiv) was added, and the reaction was stirred at rt for 4 h. The solvent was evaporated under reduced pressure. Then, the crude product was dissolved in  $\text{CH}_2\text{Cl}_2$  (20 mL) and stirred over an excess of  $\text{K}_2\text{CO}_3$  (0.83 g, 6 mmol). After 2 h, the solution was filtered and evaporated. The slurry containing product and  $\text{K}_2\text{CO}_3$  could be carried directly through to the next step (assuming 100% deprotected amine). Then, the mixture was dissolved in DMF (2 mL) under  $\text{N}_2$  atmosphere. KI (0.312 g, 1.88 mmol, 2.89 equiv), DIPEA (0.71 mL, 4.10 mmol, 6.3 equiv), and *tert*-butyl bromoacetate (0.315 mL, 2.14 mmol, 3.3 equiv) were added, and the reaction mixture was stirred at rt for 18 h. Then, the solution was diluted with  $\text{CH}_2\text{Cl}_2$  (20 mL) and washed with saturated  $\text{K}_2\text{CO}_3$  (2  $\times$  5 mL) and brine (1  $\times$  5 mL). The organic layer was dried over  $\text{MgSO}_4$ , filtered, and evaporated under reduced pressure. Purification by column chromatography (1:3 to 1:1 mixtures of EtOAc/hexane) affords **7** (263 mg, 0.455 mmol, 74% yield) as a yellow oil.  $[\alpha]_{\text{D}}^{20}$ : +17 ( $c$  = 1.0,  $\text{CH}_3\text{OH}$ );  $^1\text{H}$  NMR (400 MHz,  $\text{CDCl}_3$ ):  $\delta$  1.43 (m, 29H, 'Bu,  $\text{H}_3$ ,  $\text{H}_4$ ), 1.82 (m, 2H,  $\text{H}_3$ ,  $\text{H}_4$ ), 3.32 (m, 3H), 3.48 (m, 5H), 3.99 (s, 3H, Me), 4.02 (m, 1H,  $\text{H}_6$ ), 4.09 (m, 1H,  $\text{H}_6'$ ), 7.80 (t, 1H,  $J$  = 7.6 Hz,  $\text{H}_8$ ), 7.91 (d, 1H,  $J$  = 7.6 Hz), 7.98 (d, 1H,  $J$  = 7.5 Hz);  $^{13}\text{C}$  NMR (100 MHz,  $\text{CDCl}_3$ ):  $\delta$  18.6, 20.5, 28.0, 28.1, 52.7, 54.1, 56.8, 61.8, 63.3, 80.6, 123.4, 126.1, 137.2, 147.0, 161.2, 165.9, 170.9; IR (ATR):  $\nu$  2978, 1722  $\text{cm}^{-1}$ ; HRMS(ESI)  $m/z$  calcd for  $\text{C}_{30}\text{H}_{47}\text{N}_3\text{O}_8\text{Na}$  [ $\text{M} + \text{Na}$ ] $^+$ : 600.3255. Found: 600.3267.

**6-[[[(1S,2S)-Cyclobutane-1,2-diyltris(carboxymethyl)azanediyl]](methylene)] picolinic acid ( $\text{H}_4$  cbddap,  $\text{H}_4(\text{L2})$ ).** A solution of compound **7** (180 mg, 0.31 mmol) was dissolved in THF/ $\text{H}_2\text{O}$  (1:1, 5 mL). Then LiOH (0.052 g, 1.25 mmol, 4 equiv) was added, and the reaction mixture was subsequently stirred at room temperature for 4 h and concentrated to dryness under reduced pressure. The resultant residue was dissolved in 4 M HCl in dioxane (8 mL) and stirred at room temperature for 18 h. The solvent was evaporated under reduced pressure. A small amount of water (2 mL) was added, and the mixture was evaporated to dryness. This process was repeated once with the addition of water and twice with an addition of diethyl ether (2 mL) to afford the desired ligand (110 mg, 0.25 mmol, 77% yield) as a yellow solid.  $^1\text{H}$  NMR (600 MHz,  $\text{D}_2\text{O}$ ):  $\delta$  1.75 (m, 2H,  $\text{H}_3$ ,  $\text{H}_4$ ), 2.06 (m, 2H,  $\text{H}_3'$ ,  $\text{H}_4'$ ), 3.76 (m, 1H), 3.75 (m, 1H), 3.83 (m, 1H), 4.00 (m, 4H), 4.16 (m, 1H), 4.32 (m, 2H,  $\text{H}_6$ ), 8.01 (d, 1H,  $J$  = 7.7 Hz), 8.28 (d, 1H,  $J$  = 6.2 Hz), 8.46 (t, 1H,  $J$  = 7.6 Hz,  $\text{H}_8$ ).  $^{13}\text{C}$  NMR (150 MHz,  $\text{D}_2\text{O}$ ):  $\delta$  17.3, 18.2, 52.0, 53.1, 53.4, 60.6, 62.3, 126.2, 129.0, 146.6, 154.0, 163.0, 168.7, 174.25. HRMS (ESI)  $m/z$  calcd for  $\text{C}_{17}\text{H}_{21}\text{N}_3\text{O}_8\text{Na}$  [ $\text{M} + \text{Na}$ ] $^+$ : 418.1226. Found: 418.1221.

**Dibenzyl [(1S,2S)-cyclobutane-1,2-diyl]dicarbamate (8).** To an ice-cooled solution of **1**<sup>10</sup> (0.160 g, 0.73 mmol) in water (30 mL) and acetone (4 mL),  $\text{NaHCO}_3$  (0.120 g, 1.45 mmol, 2 equiv) and  $\text{Na}_2\text{CO}_3$  (0.230 g, 2.20 mmol, 3 equiv) were added. The mixture was stirred until the complete dissolution of the carbonates. Then, benzyl chloroformate (0.2 mL, 1.20 mmol, 1.6 equiv) was added, and the mixture was stirred at 0  $^\circ\text{C}$  (reaction was monitored by thin-layer chromatography (TLC)). After 18 h, the reaction was extracted with EtOAc (4  $\times$  50 mL), and the organic layer was dried over magnesium sulfate. The solvent was removed under vacuum, and the excess of benzyl chloroformate was lyophilized. The residue was purified by column chromatography (2:1 hexane–EtOAc) to afford diprotected amine **8** (0.155 g, 0.44 mmol, 60% yield) as a white solid. mp 70–73  $^\circ\text{C}$  (EtOAc);  $[\alpha]_{\text{D}} = -10.0$  ( $c$  = 1.0 in MeOH);  $^1\text{H}$  NMR (400 MHz,  $\text{CDCl}_3$ ):  $\delta$  1.54 (m, 2H,  $\text{H}_3$ ,  $\text{H}_4$ ), 2.17 (m, 2H,  $\text{H}_3$ ,  $\text{H}_4$ ), 3.93 (m, 2H,  $\text{H}_1$ ,  $\text{H}_2$ ), 5.11 (m,  $\text{CH}_2$ –Ph), 5.19 (br, 2H, NH), 7.37 (s, 10H, Ar);  $^{13}\text{C}$  NMR (100 MHz,  $\text{CDCl}_3$ ):  $\delta$  23.5 ( $\text{C}_3$ ,  $\text{C}_4$ ), 53.4 ( $\text{C}_1$ ,  $\text{C}_2$ ), 66.7 ( $\text{CH}_2$ –Ph), 128.1 (Ar), 128.5 (Ar), 136.3 (Ar), 155.6 (CO); IR (ATR):  $\nu$  3306 ( $\text{NH}_{\text{st}}$ ), 2975 ( $\text{CH}_{\text{st}}$ ), 1682 ( $\text{C}=\text{O}$ )  $\text{cm}^{-1}$ ;

HRMS(ESI):  $m/z$  calcd for  $\text{C}_{24}\text{H}_{24}\text{N}_2\text{O}_6\text{Na}$  [ $\text{M} + \text{Na}$ ] $^+$ : 377.1472. Found: 377.1466.

**Di-*tert*-butyl 2,2'-[[[(1S,2S)-cyclobutane-1,2-diyl]bis(benzyloxycarbonyl)azanediyl]] diacetate (9).** To a solution of anhydrous THF (8 mL) containing previously washed 60% NaH in mineral oil (280 mg, 7 mmol, 10 equiv), TBAI (1.55 g, 4.20 mmol, 6 equiv) was added under nitrogen atmosphere. At the same time, a solution of anhydrous THF (10 mL) containing diprotected amine **8** (250 mg, 0.70 mmol) under nitrogen atmosphere was prepared. After that, the second solution was added using a cannula connected to the first one. Finally, *tert*-butyl bromoacetate (0.620 mL, 4.20 mmol, 6 equiv) was added, and the mixture was stirred at room temperature for 24 h (reaction was monitored by TLC). Then, the reaction was quenched by adding 10 mL of water, and THF was removed under vacuum. Next, more water was added (10 mL), and the crude was extracted with dichloromethane (3  $\times$  30 mL). The organic layer was dried over magnesium sulfate, and the solvent was removed under vacuum. The residue was purified by column chromatography (3:1 hexane–EtOAc) to afford dialkylated diamine **9** (250 mg, 62% yield) as a brown oil along with the corresponding monoalkylated product (64 mg, 21% yield) that was submitted to further alkylation under similar conditions.  $[\alpha]_{\text{D}} = +2.0$  ( $c$  = 1.0 in MeOH);  $^1\text{H}$  NMR (400 MHz,  $\text{CDCl}_3$ ):  $\delta$  1.27–1.52 (m, 18H, 'Bu), 1.52–1.73 (m, 2H,  $\text{H}_3$ ,  $\text{H}_4$ ), 1.94–2.13 (m, 2H,  $\text{H}_3$ ,  $\text{H}_4'$ ), 3.68–4.18 (m, 4H,  $\text{H}_5$ ), 4.37–4.60 (m, 2H,  $\text{H}_1$ ,  $\text{H}_2$ ), 5.12 (m, 4H,  $\text{CH}_2$ –Ph), 7.33 (m, 10H, Ar); IR (ATR):  $\nu$  2978 (CHst), 1743 ( $\text{C}=\text{O}$ ), 1709 ( $\text{C}=\text{O}$ )  $\text{cm}^{-1}$ ; HRMS(ESI):  $m/z$  calcd for  $\text{C}_{24}\text{H}_{24}\text{N}_2\text{O}_6\text{Na}$  [ $\text{M} + \text{Na}$ ] $^+$ : 605.2833. Found: 605.2830.

**Dimethyl 6,6'-[[[(1S,2S)-cyclobutane-1,2-diyl]bis(2-*tert*-butoxy-2-oxoethyl)azane-diyl]]bis(methylene)] dipicolinate (11).** Dialkylated diamine **9** (230 mg, 0.73 mmol), KI (365 mg, 2.20 mmol, 1.5 equiv), and methyl 6-(chloromethyl)picolinate, **10**,<sup>35</sup> (300 mg, 1.60 mmol, 1.1 equiv) were dissolved in anhydrous DMF (10 mL) under nitrogen atmosphere. After that, DIPEA (0.820 mL, 4.70 mmol, 3.2 equiv) was added, and the reaction was stirred at room temperature for 30 h. Then, EtOAc (30 mL) was added, and washes with saturated  $\text{NaHCO}_3$  (3  $\times$  20 mL), brine (3  $\times$  20 mL), and water (1  $\times$  20 mL) were performed. The final organic layer was dried over magnesium sulfate, and the solvent was removed under vacuum. The residue was purified by column chromatography over silica gel with a gradient of solvents (3:1 to 1:1 mixtures of hexane–EtOAc) to afford **11** (270 mg, 0.42 mmol, 57% yield) as a brown oil.  $[\alpha]_{\text{D}} = +18.0$  ( $c$  = 1.0 in MeOH);  $^1\text{H}$  NMR (400 MHz,  $\text{CDCl}_3$ ):  $\delta$  1.39 (s, 18H, 'Bu), 1.41–1.50 (m, 2H,  $\text{H}_{4\text{R}}$ ,  $\text{H}_{3\text{S}}$ ), 1.73–1.89 (m, 2H,  $\text{H}_{4\text{S}}$ ,  $\text{H}_{3\text{R}}$ ), 3.25 (s, 4H,  $\text{H}_5$ ), 3.41 (m, 2H,  $\text{H}_1$ ,  $\text{H}_2$ ), 3.98 (s, 6H, Me), 4.05 (s, 4H,  $\text{H}_6$ ), 7.73 (m, 2H, Ar), 7.86 (m, 2H, Ar), 7.96 (m, 2H, Ar);  $^{13}\text{C}$  NMR (100 MHz,  $\text{CDCl}_3$ ):  $\delta$  19.3 ( $\text{C}_3$ ,  $\text{C}_4$ ), 28.1 ( $\text{CH}_3$ – $^t\text{Bu}$ ), 52.8 ( $\text{CH}_3$ ), 53.8 ( $\text{C}_5$ ), 57.0 ( $\text{C}_6$ ), 62.6 ( $\text{C}_1$ ,  $\text{C}_2$ ), 80.8 ( $\text{C}^t\text{Bu}$ ), 123.4 (Ar), 126.2 (Ar), 137.2 (Ar), 147.1 (Ar), 161.3 (Ar), 165.9 (CO), 170.8 (CO); IR (ATR):  $\nu$  2977 (CHst), 2951 (CHst), 1721 ( $\text{C}=\text{O}$ ), 1589 ( $\text{C}=\text{O}$ )  $\text{cm}^{-1}$ ; HRMS (ESI):  $m/z$  calcd for  $\text{C}_{24}\text{H}_{24}\text{N}_2\text{O}_6\text{Na}$  [ $\text{M} + \text{Na}$ ] $^+$ : 613.3232. Found: 613.3231.

**6,6'-[[[(1S,2S)-Cyclobutane-1,2-diyl]bis(carboxymethyl)azanediyl]]bis(methylene)] dipicolinic Acid ( $\text{H}_4$ cbddadpa,  $\text{H}_4(\text{L3})$ ).** Compound **11** (150 mg, 0.245 mmol) was dissolved in THF/ $\text{H}_2\text{O}$  (1:1, 5 mL), LiOH (31.0 mg, 0.740 mmol, 3 equiv) was added, and the reaction mixture was stirred at room temperature for 4 h. Then, the mixture was concentrated to dryness under reduced pressure, and the resultant residue was dissolved in 4 M HCl in dioxane (3 mL) and stirred at room temperature for 18 h. Then, the solvent was evaporated under reduced pressure. A small amount of water (3 mL) was added, and the mixture was evaporated to dryness. This process was repeated twice with water and twice with the addition of diethyl ether (3 mL) to afford the desired ligand (100 mg, 0.184 mmol, 75% yield) as a brown solid.  $[\alpha]_{\text{D}} = +36.0$  ( $c$  = 1.0 in  $\text{H}_2\text{O}$ );  $^1\text{H}$  NMR (400 MHz,  $\text{D}_2\text{O}$ ):  $\delta$  1.72–1.82 (m, 2H,  $\text{H}_{4\text{R}}$ ,  $\text{H}_{3\text{S}}$ ), 2.04–2.17 (m, 2H,  $\text{H}_{4\text{S}}$ ,  $\text{H}_{3\text{R}}$ ), 3.71–3.91 (m, 4H,  $\text{H}_5$ ), 4.16 (m, 2H,  $\text{H}_1$ ,  $\text{H}_2$ ), 4.46 (s, 4H,  $\text{H}_6$ ), 7.76 (m, 2H, Ar), 8.04 (m, 2H, Ar), 8.17 (m, 2H, Ar);  $^{13}\text{C}$  NMR (100 MHz,  $\text{D}_2\text{O}$ ):  $\delta$  17.7 ( $\text{C}_3$ ,  $\text{C}_4$ ), 52.1 ( $\text{C}_5$ ), 55.1 ( $\text{C}_6$ ), 51.5 ( $\text{C}_1$ ,  $\text{C}_2$ ), 125.9 (Ar), 128.7 (Ar), 143.8 (Ar), 144.2

(Ar), 152.0 (Ar), 164.1 (CO), 171.0 (CO); IR (ATR):  $\nu$  3377 (OH<sub>st</sub>), 2945 (CH<sub>st</sub>), 1720 (C=O), 1616 (C=O) cm<sup>-1</sup>; HRMS (ESI):  $m/z$  calcd for C<sub>24</sub>H<sub>24</sub>N<sub>2</sub>O<sub>6</sub>Na [M + Na]<sup>+</sup>: 495.1486. Found: 495.1478.

**Sample Preparation of the Metal Complexes.** The ligand concentrations were determined based on pH-potentiometric titration curves. Gd<sup>3+</sup>, Zn<sup>2+</sup>, and Eu<sup>3+</sup> (for luminescence lifetimes) concentrations were determined by titrating the metal solutions with standardized Na<sub>2</sub>H<sub>2</sub>edta in urotropine buffer (pH 5.6–5.8) in the presence of xylenol orange as an indicator. The GdL complexes were prepared by mixing the ligand and the metal and adjusting the pH to 7.

Protonation constants of ligands, stability constants of complexes, and protonation constants of complexes are described and defined in eqs 3–5.

$$K_i = \frac{[H_iL]}{[H_{i-1}L][H^+]} \quad (3)$$

$$K_{ML} = \frac{[ML]}{[M][L]} \quad (4)$$

$$K_{MH_iL} = \frac{[M(H_iL)]}{[M(H_{i-1}L)][H^+]} \quad (5)$$

where [M], [L], and [ML] are the equilibrium concentrations of free metal ion, deprotonated ligand, and deprotonated complex, respectively. Experimental data were refined using the computer software Hyperquad 2008.<sup>36</sup> Species distribution plots were calculated taking the experimental constants using the computer software HySS.<sup>37</sup> The ionic product of water used at 25 °C was  $pK_w = 13.77$ , while the ionic strength was kept at 0.1 M. Fixed values were used for  $pK_w$  and total concentrations of metal, ligand, and acid.

**Kinetic Measurements.** The rates of the metal exchange reactions of [Gd(L2)]<sup>-</sup> were studied by following the formation of [Cu(L2)]<sup>-</sup> using conventional UV–vis spectrophotometry. The exchange reactions were followed at 245 nm in the pH range of 3.35–4.90. The concentration of the complex was 0.11 mM, while Cu<sup>2+</sup> ion was added at high excess (10–40 equiv) to ensure pseudo-first-order conditions. The temperature of the samples was kept at 25 °C, and the ionic strength of the solutions was kept constant by using 0.15 M NaCl. To keep the pH constant, 50 mM methylpiperazine buffer was used. The pseudo-first-order rate constants ( $k_{obs}$ ) were calculated by fitting the absorbance versus time data to the monoexponential function (eq 6).

$$A_t = (A_0 - A_e)e^{-k_{obs}t} + A_e \quad (6)$$

where  $A_0$ ,  $A_t$ , and  $A_e$  are the absorbance at time = 0 s, at time  $t$ , and at equilibrium, respectively. The fittings were performed with Origin 9.1 software by using standard least-squares procedure.

**Relaxometric Measurements.** <sup>1</sup>H NMRD profiles of aqueous 1.88 mM [Gd(L1)]<sup>-</sup>, 1.91 mM [Gd(L2)]<sup>-</sup>, and 2.13 mM [Gd(L3)]<sup>-</sup> solutions (pH = 7) were measured at 25, 37, and 50 °C on a Stellar SMARTracer Fast Field Cycling NMR relaxometer (0.00024–0.24 T, 0.01–10 MHz <sup>1</sup>H Larmor frequency) and a Bruker WP80 NMR magnet adapted to variable-field measurements (0.47–1.88 T, 20–80 MHz), controlled by the SMARTracer PC-NMR console. The temperature was controlled by a VTC91 temperature control unit and maintained by a gas flow. The temperature was determined according to previous calibration with a Pt resistance temperature probe.

To avoid any free Gd<sup>3+</sup>, some ligand excess was used (6% L1, 5% L2, and 5% L3).

**<sup>17</sup>O NMR Studies.** Variable-temperature <sup>17</sup>O NMR measurements of aqueous solutions of GdL complexes were performed on a Bruker Advanced 400 MHz spectrometer using a 10 mm broad band fluorine observation (BBFO) probe (9.4 T, 54.2 MHz) in the temperature range of 1–75 °C. The temperature was calculated according to published calibration routines with ethylene glycol and MeOH. Acidified water (HClO<sub>4</sub>, pH 3.3) was used as diamagnetic reference. Transverse <sup>17</sup>O relaxation times were obtained by the Carl-Purcell-

Meiboom-Gill spin-echo technique. To eliminate susceptibility corrections to the chemical shifts, the sample was placed in a glass sphere fixed in a 10 mm NMR tube. To improve sensitivity, H<sub>2</sub><sup>17</sup>O (10% H<sub>2</sub><sup>17</sup>O, CortecNet) was added to achieve ~1% <sup>17</sup>O content in the sample. The pH of the samples was 6.5, and the GdL complex concentrations were the following: 15.3 mmol/kg ([Gd(L1)]<sup>-</sup>), 13.7 mmol/kg ([Gd(L1)]<sup>-</sup>), and 6.46 mmol/kg ([Gd(L1)]<sup>-</sup>). To avoid any free Gd<sup>3+</sup>, some ligand excess was used (6% L1, 5% L2, and 5% L3).

**DFT Calculations.** All calculations presented in this work were performed employing DFT within the hybrid meta-generalized gradient approximation (hybrid meta-GGA), with the TPSSH exchange-correlation functional.<sup>38</sup> Geometry optimizations were conducted with the Gaussian09<sup>39</sup> program package using the large-core approximation with the quasirelativistic effective core potential proposed by Dolg et al.<sup>40</sup> and the associated [5s4p3d]-GTO valence basis set for Gd. The Standard 6-311G(d,p) basis set was used for all other atoms. Bulk water solvent effects were included by using the integral equation formalism variant of the polarizable continuum model (IEFPCM),<sup>41</sup> using the universal force field (UFF)<sup>42</sup> radii scaled by a factor of 1.1 to construct the solute cavity. Analytical second derivatives were calculated to confirm that the optimized geometries correspond to local energy minima on the potential energy surface.

Hyperfine coupling constants  $A/\hbar$  were computed using the all-electron calculations with the second-order Douglas-Kroll-Hess (DKH2) method<sup>43</sup> as implemented in ORCA (release 4.0.1.2).<sup>44</sup> The basis sets used for these calculations included the SARC2-DKH-QZVP basis set for Gd<sup>45</sup> and the DKH-def2-TZVP basis set for all other atoms.<sup>46</sup> The RJCOSX approximation<sup>47</sup> was employed to accelerate the calculations using the SARC2-DKH-QZVP/JK auxiliary basis sets for Gd and auxiliary basis sets for all other atoms generated automatically by ORCA using AutoAux procedure.<sup>48</sup> Solvent effects were introduced with the universal solvation model based on solute electron density and on a continuum model (SMD).<sup>49</sup>

## ■ ASSOCIATED CONTENT

### § Supporting Information

The Supporting Information is available free of charge on the ACS Publications website at DOI: 10.1021/acs.inorgchem.9b02044.

<sup>1</sup>H and <sup>13</sup>C NMR spectra of the new products, HRMS spectra of the gadolinium complexes, potentiometry studies, details on kinetic inertness studies, anion binding studies, luminescence studies, equations used for the analysis of the <sup>17</sup>O and NMRD data, references, optimized Cartesian coordinates of the complexes obtained with DFT calculations (PDF)

## ■ AUTHOR INFORMATION

### Corresponding Authors

\*E-mail: carlos.platas.iglesias@udc.es. (C.P.-I.)

\*E-mail: eva.jakabtoth@cnrs.fr. (É.T.)

\*E-mail: rosa.ortuno@uab.es. (R.M.O.)

### ORCID

Rosa M. Ortuno: 0000-0001-7635-7354

### Notes

The authors declare no competing financial interest.

## ■ ACKNOWLEDGMENTS

O.P.-T. and J.A.O. thank Univ. Autònoma de Barcelona for predoctoral fellowships and O.P.-T. also for a travel grant. Financial support from Spanish Ministerio de Economía y Competitividad (Grant No. CTQ2016-77978-R, AEI/FEDER, UE) is gratefully acknowledged. Authors thank A. Martínez-



Hernández for her assistance in the preparation of some gadolinium complexes. C.P.-I. and D.E.-G. thank Centro de Supercomputación de Galicia for providing the supercomputing facilities.

## REFERENCES

- (1) (a) *The Chemistry of Contrast Agents in Medical Magnetic Resonance Imaging*, 2nd ed.; Merbach, A., Helm, L., Tóth, É., Eds.; Wiley: Weinheim, Germany, 2013. (b) *Theranostics and Image Guided Drug Delivery*; Thanou, M., Ed; RSC: Cambridge, UK, 2018.
- (2) (a) Sarka, L.; Burai, L.; Brucher, E. The Rates of the Exchange Reactions between  $[\text{Gd}(\text{DTPA})]^{2-}$  and the Endogenous Ions  $\text{Cu}^{2+}$  and  $\text{Zn}^{2+}$ : A Kinetic Model for the Prediction of the Magnetic Resonance Imaging. *Chem. - Eur. J.* **2000**, *6*, 719–724. (b) Pasha, A.; Tircsó, G.; Benyó, E. T.; Brucher, E.; Sherry, A. D. Synthesis and Characterization of DOTA-(amide)<sub>4</sub> Derivatives: Equilibrium and Kinetic Behavior of Their Lanthanide(III) Complexes. *Eur. J. Inorg. Chem.* **2007**, 4340–4349. (c) Pálkás, Z.; Roca-Sabio, A.; Mato-Iglesias, M.; Esteban-Gómez, D.; Platas-Iglesias, C.; De Blas, A.; Rodríguez-Blas, T.; Tóth, É. Stability, Water Exchange, and Anion Binding Studies on Lanthanide(III) Complexes with a Macrocyclic Ligand Based on 1,7-Diaza-12-Crown-4: Extremely Fast Water Exchange on the  $\text{Gd}^{3+}$  Complex. *Inorg. Chem.* **2009**, *48*, 8878–8889. (d) McMurry, T. J.; Pippin, C. G.; Wu, C.; Deal, K. A.; Brechbiel, M. W.; Mirzadeh, S.; Gansow, O. A. Physical Parameters and Biological Stability of Yttrium(III) Diethylenetriaminepentaacetic Acid Derivative Conjugates. *J. Med. Chem.* **1998**, *41*, 3546–3549. (e) Farkas, E.; Fodor, T.; Kálmán, F. K.; Tircsó, G. Equilibrium and Dissociation Kinetics of the  $[\text{Al}(\text{NOTA})]$  Complex ( $\text{NOTA} = 1,4,7$ -Triazacyclononane-1,4,7-Triacetate). *React. Kinet., Mech. Catal.* **2015**, *116*, 19. (f) Tircsó, G.; Kálmán, F. K.; Pál, R.; Varga, T. R.; Király, R.; Lázár, I.; Québatte, L.; Merbach, A. E.; Tóth, É.; Brucher, E.; et al. Lanthanide Complexes Formed with the Tri- and Tetraacetate Derivatives of Bis(aminomethyl)phosphinic Acid: Equilibrium, Kinetic and NMR Spectroscopic Studies. *Eur. J. Inorg. Chem.* **2012**, 2062–2073. (g) Rodríguez-Rodríguez, A.; Esteban-Gómez, D.; Tripier, R.; Tircsó, G.; Garda, Z.; Tóth, I.; De Blas, A.; Rodríguez-Blas, T.; Platas-Iglesias, C. Lanthanide(III) Complexes with a Reinforced Cyclam Ligand Show Unprecedented Kinetic Inertness. *J. Am. Chem. Soc.* **2014**, *136*, 17954–17957. (h) Kálmán, F. K.; Végh, A.; Regueiro-Figueroa, M.; Tóth, É.; Platas-Iglesias, C.; Tircsó, G. H4octapa: Highly Stable Complexation of Lanthanide(III) Ions and Copper(II). *Inorg. Chem.* **2015**, *54*, 2345–2356. (i) Platas-Iglesias, C.; Mato-Iglesias, M.; Djanashvili, K.; Muller, R. N.; Vander Elst, L.; Peters, J. A.; De Blas, A.; Rodríguez-Blas, T. Lanthanide Chelates Containing Pyridine Units with Potential Application as Contrast Agents in Magnetic Resonance Imaging. *Chem. - Eur. J.* **2004**, *10*, 3579–3590. (j) Phukan, B.; Malikidogo, K. P.; Bonnet, C.; Tóth, É.; Mondal, S.; Mukherjee, C. A Bishydrated, Eight-Coordinate  $\text{Gd}(\text{III})$  Complex with Very Fast Water Exchange: Synthesis, Characterization, and Phantom MR Imaging. *Chemistry Select* **2018**, *3*, 7668–7673.
- (3) Polasek, M.; Caravan, P. Is Macrocyclic a Synonym for Kinetic Inertness in  $\text{Gd}(\text{III})$  Complexes? Effect of Coordinating and Noncoordinating Substituents on Inertness and Relaxivity of  $\text{Gd}(\text{III})$  Chelates with DO3A-like Ligands. *Inorg. Chem.* **2013**, *52*, 4084–4096.
- (4) Tóth, É.; Brucher, E.; Lazar, I.; Toth, I. Kinetics of Formation and Dissociation of Lanthanide(III)-DOTA Complexes. *Inorg. Chem.* **1994**, *33*, 4070–4076.
- (5) (a) Baranyai, Z.; Brucher, E.; Uggeri, F.; Maiocchi, A.; Toth, I.; Andrási, M.; Gaspar, A.; Zekany, L.; Aime, S. The Role of Equilibrium and Kinetic Properties in the Dissociation of  $\text{Gd}[\text{DTPA-Bis}(\text{methylamide})]$  (Omniscan) at near to Physiological Conditions. *Chem. - Eur. J.* **2015**, *21*, 4789–4799. (b) Baranyai, Z.; Pálkás, Z.; Uggeri, F.; Maiocchi, A.; Aime, S.; Brucher, E. Dissociation Kinetics of Open Chain and Macrocyclic Gadolinium(III) Aminopolycarboxylate Complexes Related to Magnetic Resonance Imaging: Catalytic Effect of Endogenous Ligands. *Chem. - Eur. J.* **2012**, *18*, 16426–16435.
- (6) Tircsó, G.; Regueiro-Figueroa, M.; Nagy, V.; Garda, Z.; Garai, T.; Kálmán, F. K.; Esteban-Gómez, D.; Tóth, É.; Platas-Iglesias, C. Approaching the Kinetic Inertness of Macrocyclic Gadolinium(III)-Based MRI Contrast Agents with Highly Rigid Open-Chain Derivatives. *Chem. - Eur. J.* **2016**, *22*, 896–901.
- (7) (a) Bloembergen, N.; Morgan, L. O. Proton Relaxation Times in Paramagnetic Solutions. Effects of Electron Spin Relaxation. *J. Chem. Phys.* **1961**, *34*, 842. (b) Micskei, K.; Helm, L.; Brucher, E.; Merbach, A. E. Oxygen-17 NMR Study of Water Exchange on Gadolinium Polyaminopolycarboxylates  $[\text{Gd}(\text{DTPA})(\text{H}_2\text{O})]^{2-}$  and  $[\text{Gd}(\text{DOTA})(\text{H}_2\text{O})]^-$  Related to NMR Imaging. *Inorg. Chem.* **1993**, *32*, 3844–3850. (c) Fries, P. H.; Belorizky, E. Electronic Relaxation of Paramagnetic Metal Ions and NMR Relaxivity in Solution: Critical Analysis of Various Approaches and Application to a  $\text{Gd}(\text{III})$ -Based Contrast Agent. *J. Chem. Phys.* **2005**, *123*, 124510–124515.
- (8) Boros, E.; Caravan, P. Probing the Structure-Relaxivity Relationship of Bis-Hydrated  $\text{Gd}(\text{DOTA})$  Derivatives. *Inorg. Chem.* **2015**, *54*, 2403–2410.
- (9) (a) Gale, E. M.; Kenton, N.; Caravan, P.  $[\text{Gd}(\text{CyPic3A})(\text{H}_2\text{O})_2]^-$ : a Stable Bis(aquated) and High-Relaxivity  $\text{Gd}(\text{III})$  Complex. *Chem. Commun.* **2013**, 49, 8060–8062. (b) Bonnet, C. S.; Laine, S.; Buron, F.; Tircsó, G.; Pallier, A.; Helm, L.; Suzenet, F.; Tóth, É. A Pyridine-Based Ligand with Two Hydrazine Functions for Lanthanide Chelation: Remarkable Kinetic Inertness for a Linear, Bishydrated Complex. *Inorg. Chem.* **2015**, *54*, 5991–6003.
- (10) Sans, M.; Illa, O.; Ortuño, R. M. Stereoselective synthesis of all stereoisomers of orthogonally protected cyclobutane-1,2-diamine and some chemoselective transformations. *Org. Lett.* **2012**, *14*, 2431–2433.
- (11) Jackson, G. E.; Wynchank, S.; Woudenberg, M. Gadolinium(III) Complex Equilibria: the Implications for  $\text{Gd}(\text{III})$  MRI Contrast Agents. *Magn. Reson. Med.* **1990**, *16*, 57–66.
- (12) Kálmán, F. K.; Tircsó, G. Kinetic Inertness of the  $\text{Mn}^{2+}$  Complexes Formed with AAZTA and Some Open-Chain EDTA Derivatives. *Inorg. Chem.* **2012**, *51*, 10065–10067.
- (13) Charlier, J.; Merciny, E.; Fuger, J. Study of the complexation of trivalent lanthanides by the six isomers of diamino-cyclohexanetetraacetic acid. Part 4. Formation constants of the 1:1 complexes of four isomers and the effect of stereochemical factors on complex stability. *Anal. Chim. Acta* **1987**, *192*, 95–101.
- (14) Molnár, E.; Váradi, B.; Garda, Z.; Botár, R.; Kálmán, F. K.; Tóth, É.; Platas-Iglesias, C.; Tóth, I.; Brucher, E.; Tircsó, G. Remarkable differences and similarities between the isomeric  $\text{Mn}(\text{II})$ -*cis*- and *trans*-1,2-diaminocyclohexane-*N,N,N',N'*-tetraacetate complexes. *Inorg. Chim. Acta* **2018**, *472*, 254–263.
- (15) Pellegatti, L.; Zhang, J.; Drahos, B.; Villette, S.; Suzenet, F.; Guillaumet, G.; Petoud, S.; Tóth, É. Pyridine-Based Lanthanide Complexes: Towards Bimodal Agents Operating as Near Infrared Luminescent and MRI Reporters. *Chem. Commun.* **2008**, 60, 6591–6593.
- (16) Laine, S.; Bonnet, C. S.; Kálmán, F. K.; Garda, Z.; Pallier, A.; Caillé, F.; Suzenet, F.; Tircsó, G.; Tóth, É.  $\text{Mn}^{2+}$  complexes of open-chain ligands with a pyridine backbone: less donor atoms lead to higher kinetic inertness. *New J. Chem.* **2018**, *42*, 8012–8020.
- (17) Horrocks, W. D., Jr.; Sudnick, D. R. Lanthanide Ion Probes of Structure in Biology. Laser-Induced Luminescence Decay Constants Provide a Direct Measure of the Number of Metal-Coordinated Water Molecules. *J. Am. Chem. Soc.* **1979**, *101*, 334–340.
- (18) Horrocks, W. D., Jr.; Sudnick, D. R. Lanthanide Ion Luminescence Probes of the Structure of Biological Macromolecules. *Acc. Chem. Res.* **1981**, *14*, 384–392.
- (19) Beeby, A.; Clarkson, I. M.; Dickens, R. S.; Faulkner, S.; Parker, D.; Royle, L.; de Sousa, A. S.; Williams, J. A. G.; Woods, M. Non-Radiative Deactivation of the Excited States of Europium, Terbium and Ytterbium Complexes by Proximate Energy-Matched OH, NH and CH Oscillators: an Improved Luminescence Method for Establishing Solution Hydration States. *J. Chem. Soc., Perkin Trans. 2* **1999**, *2*, 493–504.



- (20) Supkowski, R. M.; Horrocks, W. D., Jr. On the Determination of the Number of Water Molecules,  $q$ , Coordinated to Europium(III) Ions in Solution from Luminescence Decay Lifetimes. *Inorg. Chim. Acta* **2002**, *340*, 44–48.
- (21) Aime, S.; Barge, A.; Botta, M.; Howard, J. A. J.; Kataký, R.; Lowe, M. P.; Moloney, J. M.; Parker, D.; de Sousa, A. S. Dependence of the Relaxivity and Luminescence of Gadolinium and Europium Amino-Acid Complexes on Hydrogencarbonate and pH. *Chem. Commun.* **1999**, *2*, 1047–1048.
- (22) Botta, M.; Aime, S.; Barge, A.; Bobba, G.; Dickens, R. S.; Parker, D.; Terreno, E. Ternary Complexes between Cationic Gd<sup>III</sup> Chelates and Anionic Metabolites in Aqueous Solution: An NMR Relaxometric Study. *Chem. - Eur. J.* **2003**, *9*, 2102–2109.
- (23) Aime, S.; Gianolio, E.; Terreno, E.; Giovenzana, G. B.; Pagliarin, R.; Sisti, M.; Palmisano, G.; Botta, M.; Lowe, M. P.; Parker, D. Ternary Gd(III)-L-HSA Adducts: Evidence for the Replacement of Inner-Sphere Water Molecules by Coordinating Groups of the Protein. Implications for the Design of Contrast Agents for MRI. *JBIC, J. Biol. Inorg. Chem.* **2000**, *5*, 488–497.
- (24) Aime, S.; Terreno, E.; Botta, M.; Bruce, J. I.; Parker, D.; Mainero, V. Modulation of the Water Exchange Rates in [Gd-DO3A] Complex by Formation of Ternary Complexes with Carboxylate Ligands. *Chem. Commun.* **2001**, *1*, 115–116.
- (25) Mato-Iglesias, M.; Roca-Sabio, A.; Pálincás, Z.; Esteban-Gomez, D.; Platas-Iglesias, C.; Tóth, É.; De Blas, A.; Rodríguez-Blas, T. Complexes Based on a 1,7-Diaza-12-Crown-4 Platform Containing Picolinate Pendants: A New Structural Entry for the Design of Magnetic Resonance Imaging Contrast. *Inorg. Chem.* **2008**, *47*, 7840–7851.
- (26) de Sousa, P. L.; Livramento, J. B.; Helm, L.; Merbach, A. E.; Mème, W.; Doan, B. T.; Beloeil, J. C.; Prata, M. I. M.; Santos, A. C.; Geraldès, C. F. G.; Tóth, É. In Vivo MRI Assessment of a Novel Gd<sup>III</sup>-Based Contrast Agent Designed for High Magnetic Field Applications. *Contrast Media Mol. Imaging* **2008**, *3*, 78–85.
- (27) Regueiro-Figueroa, M.; Platas-Iglesias, C. Toward the Prediction of Water Exchange Rates in Magnetic Resonance Imaging Contrast Agents: A Density Functional Theory Study. *J. Phys. Chem. A* **2015**, *119*, 6436–6445.
- (28) Bader, R. F. W.; Carroll, M. T.; Cheeseman, J. R.; Chang, C. Properties of Atoms in Molecules: Atomic Volumes. *J. Am. Chem. Soc.* **1987**, *109*, 7968–7979.
- (29) (a) Borel, A.; Helm, L.; Merbach, A. E. Molecular Dynamics Simulations of MRI Relevant Gd<sup>III</sup> Chelates: Direct Access to Outer Sphere Relaxivity. *Chem. - Eur. J.* **2001**, *7*, 600–610. (b) Lopez-Vidal, E. M.; Regueiro-Figueroa, M.; García, M. D.; Platas-Iglesias, C.; Peinador, C.; Quintela, J. M. Probing Electrostatic Potential by NMR with the Use of a Paramagnetic Lanthanide(III) Chelate. *Inorg. Chem.* **2012**, *51*, 4429–4431.
- (30) Powell, D. H.; Dhubghaill, O. M. N.; Pubanz, D.; Helm, L.; Lebedev, Y. S.; Schlaepfer, W.; Merbach, A. E. Structural and Dynamic Parameters Obtained from <sup>17</sup>O NMR, EPR, and NMRD Studies of Monomeric and Dimeric Gd<sup>3+</sup> Complexes of Interest in Magnetic Resonance Imaging: An Integrated and Theoretically Self-Consistent Approach. *J. Am. Chem. Soc.* **1996**, *118*, 9333–9346.
- (31) Esteban-Gómez, D.; de Blas, A.; Rodríguez-Blas, T.; Helm, L.; Platas-Iglesias, C. Hyperfine Coupling Constants on Inner Sphere Water Molecules of Gd<sup>III</sup> Based MRI Contrast Agents. *ChemPhysChem* **2012**, *13*, 3640–3650.
- (32) Fries, P. H.; Belorizky, E. J. Electronic Relaxation of Paramagnetic Metal Ions and NMR Relaxivity in Solution: Critical Analysis of Various Approaches and Application to a Gd(III)-Based Contrast Agent. *J. Chem. Phys.* **2005**, *123*, 124510.
- (33) Helm, L.; Merbach, A. E. Inorganic and Bioinorganic Solvent Exchange Mechanisms. *Chem. Rev.* **2005**, *105*, 1923–1959.
- (34) Baranyai, Z.; Botta, M.; Fekete, M.; Giovenzana, G. B.; Negri, R.; Tei, L.; Platas-Iglesias, C. Ligand Denticity Leading to Improved Thermodynamic and Kinetic Stability of the Gd<sup>3+</sup> Complex: The Strange Case of OBETA. *Chem. - Eur. J.* **2012**, *18*, 7680–7685.
- (35) Sun, Y.-Y.; Yi, J.; Lu, X.; Zhang, Z.-Q.; Xiao, B.; Fu, Y. Cu-Catalyzed Suzuki-Miyaura Reactions of Primary and Secondary Benzyl Halides with Arylboronates. *Chem. Commun.* **2014**, *50*, 11060–11062.
- (36) Gans, P.; Sabatini, A.; Vacca, A. Investigation of Equilibria in Solution. Determination of Equilibrium Constants with the HYPERQUAD Suite of Programs. *Talanta* **1996**, *43*, 1739–1753.
- (37) Alderighi, L.; Gans, P.; Ienco, A.; Peters, D.; Sabatini, A.; Vacca, A. Hyperquad Simulation and Speciation (HySS): a Utility Program for the Investigation of Equilibria Involving Soluble and Partially Soluble Species. *Coord. Chem. Rev.* **1999**, *184*, 311–318.
- (38) Tao, J. M.; Perdew, J. P.; Staroverov, V. N.; Scuseria, G. E. Climbing the Density Functional Ladder: Nonempirical Meta-Generalized Gradient Approximation Designed for Molecules and Solids. *Phys. Rev. Lett.* **2003**, *91*, 146401.
- (39) Frisch, M. J.; Trucks, G. W.; Schlegel, H. B.; Scuseria, G. E.; Robb, M. A.; Cheeseman, J. R.; Scalmani, G.; Barone, V.; Mennucci, B.; Petersson, G. A.; Nakatsuji, H.; Caricato, M.; Li, X.; Hratchian, H. P.; Izmaylov, A. F.; Bloino, J.; Zheng, G.; Sonnenberg, J. L.; Hada, M.; Ehara, M.; Toyota, K.; Fukuda, R.; Hasegawa, J.; Ishida, M.; Nakajima, T.; Honda, Y.; Kitao, O.; Nakai, H.; Vreven, T.; Montgomery, J. A., Jr.; Peralta, J. E.; Ogliaro, F.; Bearpark, M.; Heyd, J. J.; Brothers, E.; Kudin, K. N.; Staroverov, V. N.; Kobayashi, R.; Normand, J.; Raghavachari, K.; Rendell, A.; Burant, J. C.; Iyengar, S. S.; Tomasi, J.; Cossi, M.; Rega, N.; Millam, J. M.; Klene, M.; Knox, J. E.; Cross, J. B.; Bakken, V.; Adamo, C.; Jaramillo, J.; Gomperts, R.; Stratmann, R. E.; Yazyev, O.; Austin, A. J.; Cammi, R.; Pomelli, C.; Ochterski, J. W.; Martin, R. L.; Morokuma, K.; Zakrzewski, V. G.; Voth, G. A.; Salvador, P.; Dannenberg, J. J.; Dapprich, S.; Daniels, A. D.; Farkas, Ö.; Foresman, J. B.; Ortiz, J. V.; Cioslowski, J.; Fox, D. J. *Gaussian 09*, Revision E.01; Gaussian, Inc.: Wallingford, CT, 2009.
- (40) Dolg, M.; Stoll, H.; Savin, A.; Preuss, H. Energy-Adjusted Pseudopotentials for the Rare Earth Elements. *Theor. Chim. Acta* **1989**, *75*, 173–194.
- (41) Tomasi, J.; Mennucci, B.; Cammi, R. Quantum Mechanical Continuum Solvation Models. *Chem. Rev.* **2005**, *105*, 2999–3093.
- (42) Rappe, A. K.; Casewit, C. J.; Colwell, K. S.; Goddard III, W. A.; Skiff, W. M. UFF, a Full Periodic Table Force Field for Molecular Mechanics and Molecular Dynamics Simulations. *J. Am. Chem. Soc.* **1992**, *114*, 10024–10035.
- (43) (a) Barysz, M.; Sadlej, A. J. Two-Component Methods of Relativistic Quantum Chemistry: from the Douglas-Kroll Approximation to the Exact Two-Component Formalism. *J. Mol. Struct.: THEOCHEM* **2001**, *573*, 181–200. (b) Reiher, M. Douglas-Kroll-Hess Theory: a Relativistic Electrons-Only Theory for Chemistry. *Theor. Chem. Acc.* **2006**, *116*, 241–252.
- (44) Neese, F. The ORCA program system. *Wiley Interdiscip. Rev.: Comput. Mol. Sci.* **2012**, *2*, 73–78.
- (45) Aravena, D.; Neese, F.; Pantazis, D. A. Improved Segmented All-Electron Relativistically Contracted Basis Sets for the Lanthanides. *J. Chem. Theory Comput.* **2016**, *12*, 1148–1156.
- (46) (a) Weigend, F.; Ahlrichs, R. Balanced Basis Sets of Split Valence, Triple Zeta Valence and Quadruple Zeta Valence Quality for H to Rn: Design and Assessment of Accuracy. *Phys. Chem. Chem. Phys.* **2005**, *7*, 3297–3305. (b) Pantazis, D. A.; Chen, X.-Y.; Landis, C. R.; Neese, F. All-Electron Scalar Relativistic Basis Sets for Third-Row Transition Metal Atoms. *J. Chem. Theory Comput.* **2008**, *4*, 908–919.
- (47) (a) Neese, F.; Wennmohs, F.; Hansen, A.; Becker, U. Efficient, Approximate and Parallel Hartree-Fock and Hybrid DFT Calculations. A ‘Chain-of-Spheres’ Algorithm for the Hartree-Fock Exchange. *Chem. Phys.* **2009**, *356*, 98–109. (b) Izsak, R.; Neese, F. An Overlap Fitted Chain of Spheres Exchange Method. *J. Chem. Phys.* **2011**, *135*, 144105. (c) Petrenko, T.; Kossmann, S.; Neese, F. Efficient Time-Dependent Density Functional Theory Approximations for Hybrid Density Functionals: Analytical Gradients and Parallelization. *J. Chem. Phys.* **2011**, *134*, 054116. (d) Kossmann, S.; Neese, F. Comparison of Two Efficient Approximate Hartree-Fock Approaches. *Chem. Phys. Lett.* **2009**, *481*, 240–243.

- (48) Stoychev, G. L.; Auer, A. A.; Neese, F. Automatic Generation of Auxiliary Basis Sets. *J. Chem. Theory Comput.* **2017**, *13*, 554–562.
- (49) Marenich, A. V.; Cramer, C. J.; Truhlar, D. G. Universal Solvation Model Based on Solute Electron Density and on a Continuum Model of the Solvent Defined by the Bulk Dielectric Constant and Atomic Surface Tensions. *J. Phys. Chem. B* **2009**, *113*, 6378–6396.